Surfactant-assisted liquid-phase shear exfoliation of graphene and subsequent thin film fabrication by spray deposition

Saara Elina Sirkiä

Master of Science Thesis

Supervisors: Jussi Kauppila, Jan-Henrik Smått, Jouko Peltonen

Laboratory of Physical Chemistry

Faculty of Science and Engineering

Åbo Akademi University

Autumn 2018

Abstract

Graphite is the bulk form and source material of graphene, the versatile nanomaterial which consists of a single atomically thin sheet of carbon molecules in a honeycomb structure. It has unique properties, such as high elasticity, excellent optical properties and high electron mobility. The outstanding properties of graphene has made it the object of extensive research and a potential component for novel applications in several scientific fields, such as sensing technology. The scientific interest is high not just for graphene, the monolayer sheet, but also for graphene-like materials which are a common by-product of graphene production or otherwise resemble graphene by properties or structure. Graphene can be produced in numerous ways. This thesis investigates surfactant-assisted liquid-phase shear exfoliation which derives from mechanical exfoliation.

In the thesis, graphene was exfoliated from graphite in an aqueous surfactant-graphite suspension with a rotor-stator homogeniser. The graphene dispersion was separated with centrifugation and the graphene concentration was determined with ultraviolet-visible (UV-Vis) spectroscopy. The graphene samples were examined with scanning electron microscopy (SEM) and energy dispersive X-ray spectroscopy (EDX). Thin graphene films were produced with spray deposition and the electrical conductivity of the films was determined by measuring the electrical resistivity of the films.

Both commercial graphite and graphite excavated from Finnish soil were used to study the exfoliation, four different graphite samples in total. The graphite samples differed in particle size and purity. The Finnish graphite was excavated in Haapamäki, Finland, and purified with froth flotation and chemical leaching. The quality and yield of both the commercial graphene samples and the Finnish graphene were compared. The purity level of graphite was shown not to affect the graphene yield significantly, as opposed to the graphite particle size, which showed an effect on the yield. The electrical conductivity of the graphene thin films was found to be on a good level, considering the method used to produce the thin conductive components.

Keywords: natural graphite, graphene, surfactant-assisted liquid-phase shear exfoliation, thin film fabrication

Swedish summary - svensk sammanfattning

Surfaktant-assisterad exfoliering av grafen i vätskefas och framställning av grafenfilmer med aerosol-deponering

Introduktion

Grafen är ett material med stor potential i flera tekniska tillämpningar. Grafit, grafens bulkform och utgångsmaterial, identifierades som kolets rena aggregationstillstånd redan för nästan 200 år sedan och finns i jordskorpan överallt i världen. Det finns flera potentiella grafitdepositioner i Finland som skulle kunna utnyttjas i framtiden.

Denna avhandling är en del av forskning utfört i FennoFlakes projektet vid laboratorierna för analytisk och fysikalisk kemi samt vid geologi vid Åbo Akademi. Syftet är att framställa grafen från grafit med hjälp av surfaktant-assisterad skjuvexfoliering i vätskefas. Naturliga finländska grafitprov som har utgrävts i Haapamäki, Östra Finland, och renats med olika metoder användes för att framställa grafendispersioner. Två kommersiella grafitprov användes också som referens till den finländska grafiten. Den finländska grafiten hade fördelats till två satser och renats på två olika sätt: båda satser hade renats kemiskt med natriumhydroxid- och saltsyrabehandling och den andra hade därutöver behandlats med vätefluorid för att förbättra renhetsgraden. Grafitproven jämfördes med varandra och skillnader i utbyten och kvalitet analyserades. Dessutom framställdes tunna grafenfilmer från grafendispersionerna med spray bestrykning på ett glassubstrat. Den elektriska konduktiviteten av filmerna undersöktes och grafenets potential som en konduktiv komponent evaluerades.

Grafit är ett mineralämne som består av tunna kolskikt staplade på varandra och sammanbundna med svaga van der Waals krafter. Ett enskilt kolskikt kallas för grafen. Grafen har otaliga unika egenskaper: det har bland annat en hög elasticitet, bra optiska egenskaper och en hög elektronrörlighet. Grafen är impermeabelt för gaser och har en ytterst stor aktiv ytarea tack vare dess tvådimensionella struktur.

Dessa egenskaper gör grafen till ett bra material för exempelvis tunna och flexibla sensorer.

Grafen definieras som ett material som endast består av ett lager, dvs. ett monoskikt. Också andra grafen-liknande material uppstår ofta som biprodukt när man framställer monoskiktsgrafen från grafit, till exempel dubbelskikt eller flerskiktsgrafen. Några grafen-liknande material, till exempel porös grafen, har använts som ersättande material för att överkomma grafens problematiska tendens att reaggregera till dubbel- eller flerskiktsgrafen. Inget annat material har exakt samma enastående egenskaper som monoskiktsgrafen.

Framställning av grafen

Grafen kan framställas på flera olika sätt. Den första metoden som användes av Novoselov *et al*. i 2004 var mekanisk exfoliering, där grafit stegvis skalas av med till exempel en liten spets eller tejp för att tunna ut materialet tills bara några eller ett enskilt skikt av grafen återstår. Metoden har rapporterats att kunna framställa grafenskikt med hög kvalitet (ca 10–100 μm på en lateral skala), men i relativt små mängder. Mekanisk exfoliering kan således inte konstateras att ha potential för massproduktion av grafen. Metoden har utvecklats vidare genom att flytta exfolieringsprocessen till ett vätskemedium så att grafenutbytet kan ökas lättare utan att försämra grafenets kvalitet. Olika organiska lösningsmedel, till exempel N-metyl-2-pyrrolidon, används ofta som vätskefas för att nå ett högt utbyte. Vatten skulle vara det säkraste och mest ekologiska alternativet som vätskefas. Grafen är dock hydrofobt och brukar därför reaggregera i en ren vattenlösning. Med hjälp av ytaktiva ämnen, surfaktanter, kan grafen dispergeras i vatten och bilda stabila grafendispersioner.

I avhandlingen undersöktes framställningen av grafen med surfaktant-assisterad exfoliering i vätskefas. Exfolieringen utfördes med hjälp av skjuvkrafter, som skapades men en rotor-stator -homogenisator. Som surfaktant användes natriumkolat, som är ett natriumsalt av en gallsyra och en jonisk surfaktant. Grafit-surfaktant -suspensionen omrördes med homogenisatorn för att separera grafenflaken ur grafiten med hjälp av olika krafter, bl. a. skjuvkrafter, kavitation

och partikelkollision. Suspensionen tilläts stå över natten före en separation av större partiklar och föroreningar gjordes med centrifugering så att endast grafenet återstod dispergerat i supernatanten. Dispersionen förvarades i en glasflaska och grafenkoncentrationen bestämdes med UV-Vis spektroskopi genast efter centrifugeringen. Dispersionernas stabilitet observerades genom att bestämma koncentrationen efter några dagar samt en vecka efter centrifugeringen. Grafenets kvalitet uppskattades med hjälp av svepelelektronmikroskopi (SEM) och energidispersiv röntgenspektroskopi (EDX).

På grund av dess utmärkta elektriska egenskaper, har grafen stor potential som konduktiva tunna filmer. Ett sätt att framställa sådana komponenter är att spraya grafendispersioner på ett lämpligt substrat och låta vätskan avdunsta. I avhandlingen användes grafendispersionerna för att framställa tunna filmer med hjälp av spray-deponering på ett glassubstrat. Grafenytans torkningstid förbättrades med hjälp av pyrolys genom att hetta glassubstratet på en kokplatta under sprayandet. Den elektriska konduktiviteten av filmerna bestämdes genom att mäta provens elektriska resistivitet.

Resultat och slutsatser

I avhandlingen observerades att grafenutbytet varierar mellan olika grafitprov och det verkar korrelera med provets partikelstorlek. Grafenets kvalitet evaluerades med SEM och EDX och tyvärr gjorde ett överskott av surfaktant i grafenproven SEM bilderna dimmiga och svåra att evaluera. Dialys användes för att avlägsna en del av surfaktanterna ur grafendispersionerna och de nya SEM bilderna blev klarare. Grafenytans tjocklek i SEM-proven var dock för tunn och det fanns för lite grafen i varje prov. Därutöver visade EDX-mätningarna flera olika föroreningar i proven som inte befann sig i de ursprungliga grafitproven. Inverkan av föroreningarna på grafenets kvalitet och analysens tillförlitlighet är ännu obestämda. Dock verkade inte grafiternas renhetsgrad påverka grafenutbytet lika mycket som grafits partikelstorlek.

Det högsta grafenutbytet nåddes genom att maximera både exfolieringstiden och grafitkoncentrationen. De här två parametrarna bestämdes att vara kritiska i betraktande av grafenutbytet. En större rotordiameter i mixaren, och således ett högre skjuvkraftsvärde, ökade också grafenkoncentration. Ökande centrifugeringshastighet minskade också utbytet och ökade dispersionsstabiliteten. Standardhastigheten, 1500 rpm, gav dock tillräckligt stabila dispersioner och därmed förblev det optimala värdet på centrifugeringshastigheten. Surfaktantkoncentrationens standardvärde (5 mM) förblev också det optimala värdet för processen. Grafenutbytet var också beroende på grafenets partikelstorleksfördelning, och det högsta utbytet nåddes med partiklar mellan 125 och 150 μm.

Den elektriska konduktiviteten hos de tunna grafenfilmerna evaluerades genom att mäta den elektriska resistiviteten men en multimeter. Flera försök utfördes för att kunna optimera parametrarna i spray-deponeringen. Med en hög grafenkoncentration fick man tjockare grafenfilmer under en kortare deponeringstid. Odialyserade grafenprov visade nästan ingen konduktivitet, oberoende av dispersionens grafenkoncentration. Resistivitetsvärdena minskade betydligt hos filmer framställda med dialyserade dispersioner som hade lägre grafenkoncentrationer. Dialys kan således möjligen användas för att spara utgångsmaterial och tid under exfolieringsprocessen. Resistivitetsvärdena kunde minimeras till en nivå som resulterar i en tillräckligt hög elektrisk konduktivitet för att kunna användas i tunna grafenfilmerna som elektriskt ledande material. Med hjälp av dialys kan man möjligtvis också skala upp processen från den nuvarande väldigt småskaliga 10 ml-processen till en större volym. Det är känt att grafenutbytet minskar med ökande provvolym, men med dialys kan den optimala grafenkoncentrationen minimeras och ändå framställa konduktiva filmer.

Sammanfattningsvis, fyra olika grafitprov undersöktes i avhandlingen och skillnaderna som upptäcktes mellan proven diskuterades. De kritiska processparametrarna undersöktes och optimerades enligt resultaten. Föroreningarna som hittades i grafenproven borde möjligtvis undersökas noggrannare för att bestämma dess inverkan på grafenets kvalitet. Några utvecklingspunkter, som upptäcktes under experimenten, kan fungera som bas till kommande undersökningar.

List of Figures

List of Tables

Contents

1 Introduction and aim of the thesis

Since the discovery of graphene, it has been the subject of extensive research with a goal to harness its unique properties to be used in industry. While graphite, the source material of graphene, is in commercial distribution in very pure forms, there is a growing demand for new sources of graphite which meet the demands of graphene fabrication. Natural graphite is found at numerous sites in Finland and it can be excavated and purified to be used as a natural source of graphite and as a precursor for pristine graphene.

The research performed in the FennoFlakes project at the laboratories of physical chemistry, analytical chemistry and geology at Åbo Akademi University has set the basis for this thesis. In the project, Finnish natural graphite has been procured from geological samples excavated in Haapamäki. The Haapamäki deposit is located in Eastern Finland and it is considered a promising site for graphite mining. The graphite has been ground and separated from impurities using froth flotation and chemical leaching.

In this thesis graphene fabrication by surfactant-aided shear exfoliation was studied. Finnish natural graphite and commercial graphite from two different manufacturers, Sigma Aldrich (SA) and Alfa Aesar (AA), were used to fabricate the graphene: the Sigma-Aldrich graphite has a particle size over 150 μm and the Alfa-Aesar has a small particle size, under 45 μm. The Finnish graphite had been divided into two sets based on different purification processes: the first one was subjected to NaOH and HCl leaching and the second was additionally treated with HF to achieve higher purity. The commercial graphites were used as reference materials. These four samples deviate in properties such as particle size and purity and consequently showed different behaviour during the exfoliation and separation process.

The concentrations of the graphene dispersions and the quality of the graphene produced were analysed with ultraviolet-visible (UV-Vis) spectroscopy and scanning electron microscopy/energy dispersive X-ray spectroscopy (SEM/EDX). The results of the graphene exfoliated from the Finnish graphite samples were

compared with the ones originating from commercial graphite, as well as with each other.

One aim of the thesis was to determine whether the Finnish graphite can be used to fabricate graphene dispersions with similar properties as the ones produced from commercial graphite. And yet, if the Finnish graphite samples with different levels of purity both give adequate results, then the additional purification step may be unnecessary and can be excluded in the future. The critical factors of the process were evaluated and optimised. The differences between the graphite samples and their influence on the results were discussed. In addition, thin films are fabricated from the graphene dispersions with spray deposition onto a glass substrate and the electrical conductivity of the films was determined by measuring the electrical resistivity of the films. The results were analysed and the suitability of the method for producing conducting component materials was evaluated.

2 Graphite and graphene

Carbon is a highly diverse element which can take many forms in nature. Graphite was identified, together with diamond, as a pure allotrope of carbon over 200 years ago, when Lavoisier classified carbon as an element of its own [1]. Graphite is a naturally occurring mineral and it has been listed as one of the most critical minerals by the European commission since 2010 [2]. Graphite is excavated all around the world, with the largest production rates recorded in China, India and Brazil in 2015 [3]. Graphite was also produced in Finland from 1760 until 1947. Thirty different deposits have been used in total during this time to procure natural graphite. Ten of the deposits are now located in the Russian Karelia, outside the Finnish borders. Figure 1 shows the 20 old deposits still located in Finland. Although there are no known graphite deposits in Finland which could respond to the current demand in an economically beneficial way, the potential of such discoveries has been estimated to be high [3].

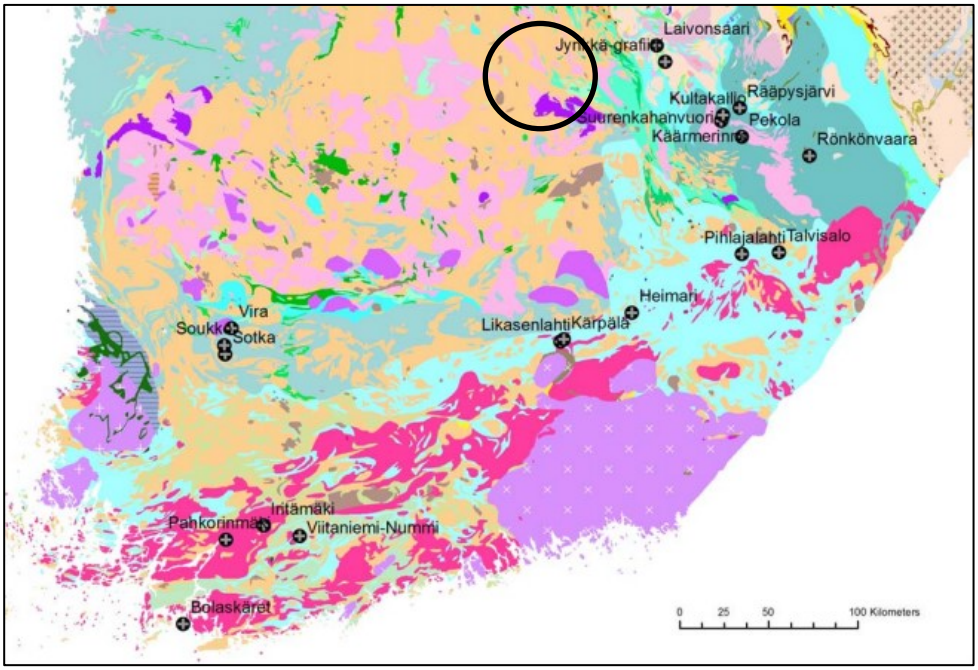

Figure 1. A geological map showing the graphite deposits (⊕) used between the years 1760-1947 in Finland. The Haapamäki study region (O) is located near the deposition cluster in the east (not included in the original image, edited in for this thesis). Image edited and published with permission from the copyright owner [3].

Graphite is a versatile material used in several industrial fields including high-technology applications, and it is the bulk form of the promising nanomaterial, graphene [1]. The first isolation of graphene from graphite was reported in 2004 by Novoselov *et al* [4,5]. Graphene has subsequently become the subject of many studies as it is a unique and promising material. However, the demand for industrial applications has and will only increase once mass-produced graphene reaches the same level of quality and unique properties as the specimens fabricated at the laboratory scale [6,7].

During the recent decades, several new allotropes of carbon (apart from graphite and diamond) have been discovered and studied. These include fullerenes, carbon nanotubes and graphene. Graphene is a basic component of the three-dimensional graphite as well the one-dimensional carbon nanotubes (CNTs). CNTs and the sphere-shaped fullerenes can hence be seen as rolled-up graphene, as shown in Figure 2, while graphite consists of numerous graphene monolayers piled on top of each other. As many other nanomaterials, graphite and graphene have experienced similar stages of discovery and development: the bulk form of the material has been already in use for hundreds of years before the discovery of its low-dimensional allotropes [1].

Graphene consists of a uniform 6-ring structure which is constructed of two symmetrical bodies by covalent σ-bonds. This structure is rich with sp^2- hybrid orbitals with delocalised electrons [8]. This unique structure is the key feature which gives graphene exceptional properties that have not been found in any other material so far. For instance, owing to its outstanding mechanical properties, graphene has been stated to be the strongest material yet to be discovered [9].

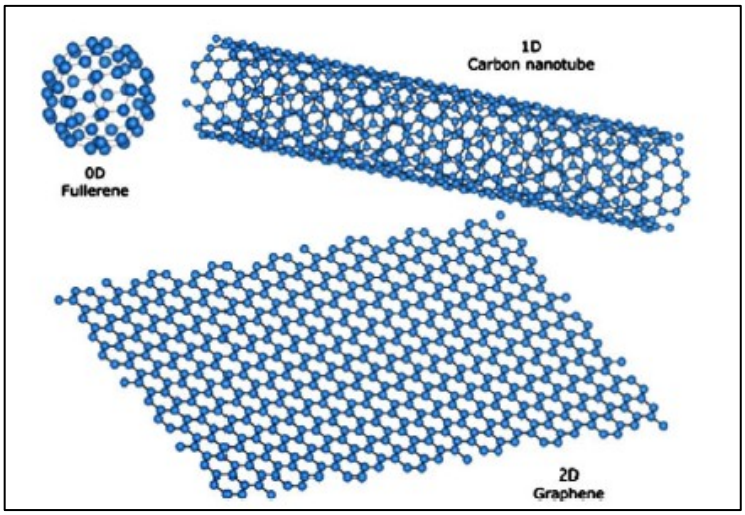

Figure 2. The low-dimensional allotropes of carbon: Fullerene (0D), CNTs (1D) and graphene (2D). Picture used with permission from the copyright owner [1].

The potential of graphene is, as mentioned, very high. The ever-increasing consumption of energy and fossil-based materials creates a need for novel materials with greater capacity for simple mass-production of products which can be used more than only once. Graphene has the potential of being used in new, lighter and more durable energy harvesting and storage devices [10].

The increase in material and energy consumption leads to - and has already led to – an increase in greenhouse gas emissions. The continuous surveillance of this phenomenon requires reusable low-cost sensors with low detection limits. Graphene-based materials can provide this with their high conductance, low Johnson noise and their suitability to be integrated into a variety of devices. These sensors can be used to detect several different gaseous compounds, e.g. the harmful yet very common emission gas, CO_2 [11].

2.1 Properties of graphene

The outstanding properties of graphene combined with its low-dimensional structure are the key factors giving rise to the large interest around the material. These properties can be utilised in several scientific fields to either enhance the performance of applications used today or to create new applications. The mechanical properties of graphene make it a potential component for flexible and wearable accessories that can be used more than once. The optical and electrical

properties of graphene make it an interesting material for different types of sensors. The next chapters discuss these three properties and their impact on the character of material. For this thesis, the most interesting attributes are the electronic properties of graphene.

2.1.1 Mechanical properties

Graphene has been shown to have exceptional mechanical properties in comparison to for example steel which has been reported as one of the strongest materials. The elastic (Young's) module of graphene has been reported to be approximately 1 TPa [12] when the corresponding value for steel is significantly lower, 210 GPa [13]. The intrinsic strength of graphene is 130 GPa, and its elastic stiffness in the second and third order are 340 N/m and -690 N/m, respectively. The breaking strength of a homogenous, undefected graphene layer has been reported to be 42 N/m. The theoretical breaking strength of a steel layer of the same thickness as monolayer graphene (3.35 Å) is 0.084-0.4 N/m, which means that graphene is around hundred times stronger than steel [14].

However, it is challenging to determine the properties of graphene exactly due to uncertainty of the geometrical dimensions of the sample and potential defects in its structure, which would influence the results. The results reported for the stiffness values of graphene show variations that may be induced by intrinsic corrugation on the graphene surface. This could be caused by stress on the boundary of the graphene sheet or so called "point defects" on the surface [15]. The mechanical properties of chemically modified graphene were studied by Gomez-Navarro *et al.* in 2008. The elastic module of graphene oxide reduced with hydrogen plasma has been reported as 0.25 TPa, which is significantly lower than the elastic module of pristine graphene [16]. New methods enable the accurate determination of sample geometry and mechanical properties. Suk *et al*. have presented a hybrid method including the determination of the mechanical properties of a graphene oxide monolayer with atomic force microscopy (AFM) and a subsequent mapping method for the determination of Young's modulus and pre-stress by finite element method (FEM). This enables the measurement of all these properties at the same time and

is predicted to be applicable for universal use, thus giving detailed information and a deeper understanding of the mechanical properties of all low-dimensional materials [17]. Due to the elastic nature of graphene, it is a suitable component material for flexible strain sensors that can be used as pressure sensors or in healthcare use in devices which can be attached to the human body for physiological monitoring purposes [18]. The gas impermeability of graphene is an excellent property considering the use of graphene in ultra-thin protective coatings, barrier films or as thin membranes in sensitive gas sensors [6,7].

The high surface area of graphene, although not technically a mechanical property, gives it an exceptionally high number of active sites for molecule adsorption. In fact, the adsorption of molecules is a key property for graphene and can be utilised in various ways, for instance to detect biological compounds in aqueous solutions. For example, the presence of antibiotics in water is very problematic for both ecological and health-related reasons. Biosensors produced with graphene can potentially be used to detect antibiotics in water through weak π-π interactions between the delocalised electrons in graphene [19].

2.1.2 Optical properties

The optical properties of graphene are, like its other properties, exceptional and widely studied. Due to the high electron mobility in graphene, it has a significant, wavelength-dependent optical absorption value ($\pi\alpha$ = 2.3 %). This property, together with the transparency of graphene at UV-range, makes graphene an interesting subject to studies involving photoelectronic applications [6].

The optical properties of graphene have been investigated by different theoretical approaches. According to Falkovsky, the optical properties of graphene are independent of the electron transport between energy bands. It has been verified through studies that the transmittance of graphene is dependent on the frequency in the visible light spectrum and takes a universal value due to its fine structure [23].

The Dirac fermions found in graphene give rise to interesting optical properties. High frequency conductivity has been observed for graphene from the IR light region all the way to the visible light spectrum. The ‘universal’ behaviour of

materials shows that the transmittance decreases with an increase in the material thickness. However, graphene does not follow this character, but shows a constant transparency (~ 97.7%) in the visible range. This is thought to be the result of low-energy photons which have been found on graphene surface [16].
Xia *et al*. have reported outstanding values of transport velocity and ultrahigh photoresponse on graphene surfaces in 2009. This means that graphene is a potential material for optoelectronic equipment used for communication and sensor technology [60]. The optical properties of graphene also enable the determination of graphene concentration in a liquid medium with UV-Vis spectroscopy.

2.1.3 Electrical properties

Graphene holds unique electronic properties due to several phenomena. It is ambipolar at room temperature, which means that its charge carriers can be changed between electrons and holes by altering the gate voltage. The sp^2- hybridization of two s-orbitals and one p-orbital enables the trigonal plane structure of graphene and its 1.42 Å σ-bands. The p-orbital has the ability to form covalent bonds with adjacent carbon atoms and thus form half-filled π-bands. These bands are characteristic for transition elements and give them notable properties, such as strong intermolecular bonds, high Coulomb energies, magnetism and isolative behaviour. Therefore, Pauling suggested in the 1950's that graphene should be classified as a resonance valence bond structure. Graphene has also been referred to as a semimetal due to the linearly dispersed electronic excitations, or Dirac electrons, found in the structure [19].
Experiments have shown that graphene has a high electron mobility of $2.5 \cdot 10^5\ \mathrm{cm^2 \cdot V^{-1} \cdot s^{-1}}$ at room temperature and a high tolerance for electric current [6]. The electronic properties of graphene can also be modified, for example by induced structural defects. Local modifications in e.g. electronic and optical properties can be created through so called "ripple engineering" and utilised in specific applications [16]. Controlled modification of graphene structure has been successfully performed by electron beam bombarding of graphene samples with increasing intensity in a scanning electron microscope (SEM) chamber. The

samples were analyzed with Raman spectroscopy afterwards for electric resistance and electron mobility. The results showed the electric current resistance of graphene to increase as the intensity of the electron beam was increased, due to destruction of bonds by the irradiation. It was also noted that the modifications on the monolayer graphene surface are reversible to some extent by e.g. storing the samples in vacuum [21].

The outstanding electrical properties of graphene make it a good candidate for nanoelectromechanical (NEMS) applications. One group of these applications is biosensors. In 2015, Li *et al*. reported a successful attempt to produce biosensors from modified graphene nanoplatelets. Polyolefins and TiO_2 was used to control the morphology of graphene and to induce the components into the material, respectively. These sensors were used to detect several types of lung cancer biomarkers [22].

Graphene is also applicable for fluorescent detection methods. Together with dyes, its high energy transfer potential can be utilised to transport the excited electrons of the dyes through the sensing material. This method is used for building FRET (fluorescent resonance energy transport) sensors. In 2010, Chang *et al*. produced a FRET sensor with thrombin to induce the detection of blood coagulation markers. This method was shown to be twice as sensitive as corresponding sensors fabricated with carbon nanotubes as a precursor [23].

Graphene-based sensors can also be used to detect harmful substances by electrochemical reactions. Zhang *et al*. described in 2016 a production process for the detection of hydrogen peroxide, which is toxic for humans, but can at times be found in food and the environment. A glass-carbon electrode was modified with a tin oxide-graphene oxide platform and used for electrochemical detection of hydrogen peroxide. The sensor showed high sensitivity and selectivity for the detection [24].

2.2 The structure of graphene and graphene-like materials

Graphene owes its outstanding properties to its unique structure. While graphene is by definition a single, two-dimensional layer of carbon atoms, there are several materials which are close to graphene by either structure or other properties. Despite the resemblance, none of the graphene-like materials have the exact properties of monolayer graphene. Numerous production methods - also the one used during this thesis - result in not just monolayer graphene, but a mixture of mono-, bi- and few-layer graphene sheets. The next chapters introduce the structure of monolayer graphene and other graphene-like materials.

2.2.1 Monolayer graphene

Monolayer graphene is a single two-dimensional layer consisting of carbon atoms. The monolayer structure is the defining attribute of graphene. It has unique electronic properties due to its extraordinary structure (see chapter 1.2.3). Its chemical and electronic properties has been accounted to wave-like rippling on the graphene surface. These ripples are usually 1 nm high corrugations on the graphene surface with characteristic 10-25 nm distances. These ripples are not essential to the structure, as it has been shown by Lui *et al.* in 2009, and can be evened out to obtain ultraflat graphene. Monolayer graphene was produced with an evened ripple structure to study the effect of the wave structure on the surface. The graphene was fabricated on a flat mica substrate and showed no more than a 25 pm variation in thickness. In addition, the experiment showed a substantial yield of graphene [25].

2.2.2 Bi- and few-layer graphene

Bilayer graphene consists of two monolayer graphene sheets piled on top of each other. Unlike monolayer graphene, bilayer graphene can be characterized as a semiconductor by its electronic properties. In addition, its Dirac fermions have a limited value for mass. The Hall effect in bilayer graphene also deviates from the corresponding phenomenon in monolayer graphene. However, it can be altered by gate voltage alteration to obtain symmetry between the two graphene layers and thus restore the semiconducting holes and the regular Hall effect [5].

Few-layer graphene (FLG) is characterized as 3 to 10 graphene layers stacked on each other and bound together by van der Waals forces. The layers of few-layer graphene can be stacked in different ways which creates different types of three-dimensional structures: hexagonal AA-stacking, Bernal- or AB-stacking or rhombohedral ABC-stacking. The structure of FLG shows no band gap and increasing metallic properties with an increase in layer number. The surface area of FLG is almost as large as that of single-layer graphene. It shows high potential for different applications, such as novel Li-ion batteries. It has shown to be easily modifiable with chemical functionalization [5].

FLG can be produced with many methods. Chemical vapour deposition is a method which involves graphene production on a suitable surface. CVD with CH_4 on a Cu-substrate has shown to be a possible method by Wang *et al* [26]. The non-soluble character of copper is beneficial to the process. The resulting FLG sheets were described as of adequate quality, but not achieving the quality of exfoliated graphene at the time [27].

Another potential method is exfoliation of graphite with ball-milling and organic solvents in a low temperature. The method has been introduced by Amiri *et al*. in 2017 and is based on the modification of the surface energies of graphene and different solvents used in the exfoliation process. According to Somayajulu correlation and the research of Mulero *et al.* [61], the surface energy of the solvent nearly equals the surface energy of graphite at -195,8 °C, the boiling temperature of liquid nitrogen. This method has been stated as the fastest known method to produce high-quality FLG without expensive instrumentation, although the mechanism has not yet been fully comprehended [28].

Shear exfoliation has also been successfully used to fabricate few-layer graphene with high quality. Paton *et al.* reported a scalable method which utilizes shear exfoliation of graphite with a rotor-stator mixer with both N-methyl-2-pyrrolidone and aqueous SC solution. It was expected that shear exfoliation takes place at turbulent regions in the mixing, but the experiments showed that graphene is also sheared off graphite in regions of partial or no turbulence. On the other hand, it was discovered that exfoliation of graphene occurred at a shear rate of $\dot{\gamma}_{min} < 10^4\ s^{-1}$, regardless of the instrument used. The scalability was determined to be controlled mainly by five mixing parameters: the rotor diameter, graphite concentration, exfoliation time, liquid volume and the rotor speed. It was shown through modelling and experiments that the process has potential for scale-up and extremely high yields of graphene dispersions [36].

2.2.3 Graphene oxide

One of the first methods involving liquid exfoliation of graphite was the oxidisation of graphite. In 2006, Ruoff *et al*. presented the production of monolayer graphite oxide, now known as graphene oxide [29]. Graphene oxide is a very popular precursor for production of graphene and graphene-like materials due to the simplicity of the fabrication methods and its ability to form stable dispersions in water solutions. Its water-solubility comes from oxygen sites on the surface which promote a negative charge on the graphene oxide surface [30].

The source material for graphene oxide is graphite, which is first oxidised with for example $KMnO_4$ and H_2SO_4 (Hummer's method) and subsequently exfoliated in the liquid phase. The exfoliation of graphite oxide can be performed with for example mixing or sonication [16]. Due to the presence of oxide groups, graphene oxide is not electrically conductive and is therefore not useful in several applications where conductive graphene components are needed [31]. Graphene oxide can also be reduced after fabrication with e.g. $NaBH_4$ or electrochemical reduction, thus eliminating the oxide groups. High-purity graphene has been successfully fabricated with thermal reduction of graphene oxide. In fact, graphene fabrication from graphene oxide is a cost-effective and popular method to mass-

produce graphene. Reduced graphene oxide has indeed shown to be a well-suited precursor for graphene-based sensors [16]. Although there are studies suggesting that the reduction process is never complete, the method is studied extensively for pristine graphene fabrication [7].

Graphene oxide has also been used as a precursor for 3-D graphene foam. Graphene foam has been found to function well as a component for energy storage in micro-supercapacitators. Graphene foam was shown to have high electric conductivity and superior capacitance. The material also shows good contact with the electrolytes due to the micropores in the foam and therefore enables fast transport of electrolytes in the material [32].

2.2.4 Porous graphene

Porous graphene is not exactly a subtype of graphene, but a nanoporous material which is similar to graphene. Porous graphene has been offered as an advantageous alternative to graphene, which tends to restack into graphite due to the van der Waals forces. The production of porous graphite is cost-effective and environmentally friendly, and the resulting material has shown to have excellent electrochemical properties and a high surface area [33].

The pore size of porous graphene depends on the fabrication technique used, and it can range from atomic dimensions up to nanoscale. The pore structure affects the properties of porous graphene and consequently its potential applications. Porous graphene has shown to possess quite different properties from traditional graphene and holds potential for several applications in e.g. energy storage, gas purification and DNA-sequencing [34].

The key properties of porous graphene – pore size together with pore size distribution – vary depending on both fabrication method and fabrication circumstances. In 2009, Bieri *et al*. succeeded in producing two-dimensional polyphenylene which was characterized as porous graphene with scanning tunneling microscopy. The pore size was determined to be 2.48 Å. Porous graphene has also been fabricated by Fischbein *et al*. [62] using transmission electron

microscopy to drill nano-sized holes into graphene. The method was reported as repeatable and effective despite some damage observed around the pores [34].

3 Fabrication of graphene

The synthesis of monolayer graphene has been studied already since the 1970's. However, the first successful experiment to isolate a graphene layer was not reported until 2004 by Novoselov *et al*. The first fabrication method used was mechanical exfoliation of graphene from graphite. Many other methods have been studied and developed since then. These methods can be roughly divided into two groups (examples listed below):

Top-down:
Mechanical exfoliation [29]
Shear exfoliation [36]
Chemical exfoliation [16]
Electrochemical exfoliation [59]
Ball-milling [28]
Sonication [16]

Bottom-up:
Epitaxial growth, e.g. CVD [16]

The top-down approaches involve isolation of the graphene layer from a larger graphite body, and in bottom-up approaches the graphene layer is built up at atomic level [5]. Although the demand for pristine graphene is high and several fabrication methods have already been discovered, two challenges remain: the control over the amount of the graphene layers produced and the control over the uniformity of the produced graphene layer. In addition, the methods used should be applicable for mass production [35]. This thesis discusses surfactant-assisted liquid-phase shear exfoliation. The method is a derivative of mechanical exfoliation and belongs to the group of top-down approaches.

3.1 Mechanical exfoliation

As mentioned, mechanical exfoliation of graphene from graphite was the first method which was reported as a repeatable graphene synthesis method in 2004. In principle, mechanical exfoliation breaks the weak van der Waals forces holding the graphene layers together in the graphite [5]. In practice, the first mechanical exfoliation method involved stepwise exfoliation of graphite with regular tape to thin out the graphite until only a few, or one, graphene layer is left. The result of the exfoliation was observed with optical microscopy and the exfoliated layers were transferred from the tape onto a substrate. One disadvantage of the method is the contamination of the sample by the glue in the tape. The contact with glue has been eliminated by attempting graphene deposition onto a substrate by applying high voltage to the graphite sample. The method yielded small amounts of few-layer graphene on a silica substrate with a relatively non-uniform thickness. The yield was improved by aiding agents, such as sodium ions in borosilicate, which lead to anodic bonding of the cations from bulk materials onto the substrate surface which is induced by both applied voltage and heating. Subsequent thinning of the sample with tape resulted in ultra-thin layers of graphite [7]. These methods have been reported to produce graphene with good quality, but in relatively small areas (appr. 10-100 μm in lateral dimensions). Hence, mechanical exfoliation cannot be considered as a potential method for mass production of graphene [16].

3.2 Surfactant-assisted liquid-phase shear exfoliation of graphene

Due to the previously named issues concerning mechanical exfoliation, other methods have been considered for mass production of high-quality graphene. One of these is liquid-phase exfoliation, where the physical forces are induced into a liquid-graphite suspension aiming to disperse the sheared graphene flakes into the medium. The method is well applicable for applications in need of components with

good electrical properties, and the liquid medium enables the use of graphene in applications such as printable electronic sensors [29,36].

In 2008, the first results on successful, high-yield liquid-phase exfoliation of graphene were published. Hernandez *et al.* showed that graphite powder can be exfoliated to produce stable graphene dispersions in organic solvents [66]. In the same year, Blake *et al*. succeeded in their efforts to produce liquid-phase monolayer graphene with ultrasonication. Experiments with different solvents revealed that liquid-phase exfoliation is possible only with solvents with a surface tension value of approximately 40 mJ/m [29]. Although sonication is a widely-studied method which gives defect-free graphene, the method also has scalability issues as a major disadvantage [36].

Along with sonication, liquid-phase exfoliation can be carried out using mechanical forces. Shear exfoliation is a mixing method where the shear force is created with a bladed agitator. One popular shear exfoliation instrument is a rotor-stator homogeniser, where the shearing takes place between the high-speed rotor and the stationary cylinder, stator. The main energy dissipation areas – hole region, rotor swept region and jet region - are located between the rotor and the stator. In the energy dissipation regions, the homogeniser shears the graphene sheets off the graphite particles with different forces such as shear force, jet cavitation (as the fluid jets out of the stator holes with high speed) and random particle collision. A dispersing head for a Polytron rotor-stator homogenizer, which was used for shear exfoliation in this thesis, is presented in Figure 3. Together with centrifugation to separate the unexfoliated graphite from the graphene, shear exfoliation produces a dispersion of mono-, bi- and few-layer graphene [37].

Figure 3. Dispersing head for Polytron® rotor-stator homogeniser. Image used with permission from the owner [38].

Popular solvents for liquid-phase shear exfoliation include N-methyl-2-pyrrolidinone, which has been discovered to give high graphene concentrations, up to 2 mg/ml [39]. Water would be the most ecological and the safest choice for a solvent, yet the surface tension specification rules out pure water as an optimal solvent, as its surface tension is approximately 72 mJ/m. The use of water as a solvent in liquid-phase exfoliation leads to the reaggregation of graphene layers due to electrostatic effects. This phenomenon can be hindered using an aqueous surfactant solution instead of pure water as the liquid phase [29]. One such compound is sodium cholate (SC) which was studied in this thesis. An exfoliation method free of both surfactants and sonication has recently been reported as successful and reliable, but it requires surface modifications of the graphene layers with OH^- ions, which compromises the pristine nature of graphene [40].

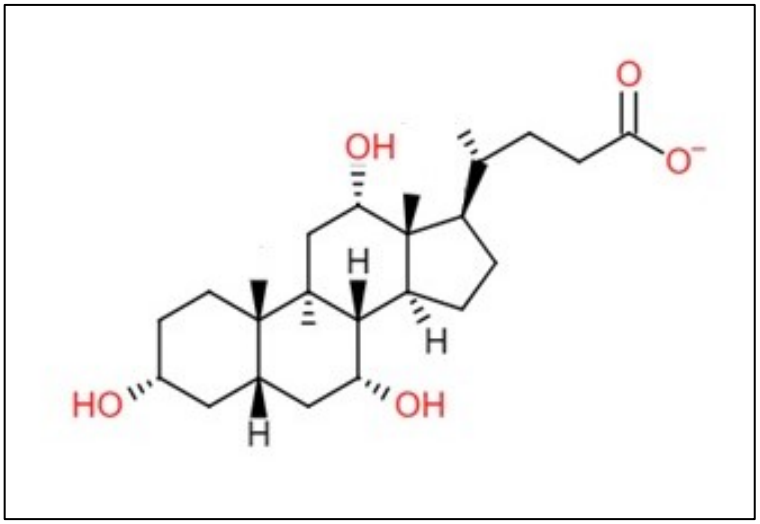

Figure 4. The molecular structure of a cholate ion.

SC, a bile acid salt, is a widely used biological surfactant which has a remarkable ability to disperse e.g. non-water-soluble cholesterols in living cells. This ability is due to the structure of SC (cholate ion presented in Figure 4) which consists of a unique, rigid steroid ring frame. The compound has an amphiphilic character caused by the hydroxyl groups and the charged carboxylate group in one end (hydrophilicity) and the methyl groups on the carbon frame (hydrophobicity) [41]. The effects of the surfactant may not all be positive. The presence of the surfactant may induce changes in the properties of the resulting graphene. It has been stated

by Shih *et al*. in 2012 that the presence of a surfactant affects the carrier transport properties of graphene in several ways [42]. The group compared graphene fabricated with conventional mechanical exfoliation and graphene produced with surfactant-assisted liquid-phase exfoliation, and their carrier transport behaviour varied significantly. They observed a hysteresis in gate voltage sweep which was reported to be independent of both sweeping speed and the voltage range. In addition, a significant reduction in both electron mobility and minimum conductivity were observed when comparing the mechanically exfoliated graphene to the surfactant-doped graphene. This can be caused by the adsorbed surfactant molecules on the graphene surface, which can alter or even hinder the carrier transport. However, the effect of the molecular structure of the surfactant on the carrier transport is not yet well-known [42], although the molecular structures of most common surfactants differ significantly from each other.

Liquid-phase exfoliation is a simple process that can be carried out without any expensive instrumentation, given that the conditions for exfoliation are optimal. In 2014, Yi *et al*. reported a successful exfoliation of few-layer graphene from graphite crystals using a conventional kitchen blender to induce exfoliation using N,N-dimethylformamide as solvent. The resulting graphene was studied extensively (using e.g. Raman, FTIR and XPS) and it was found that the product was high-quality few-layer graphene which had not been chemically functionalised during the exfoliation [43].

3.3 Qualitative analysis of graphene with SEM and EDX

SEM imaging is used for analysing a variety of graphene sample attributes. One aim is to characterise the layer structure in for example few-layer graphene [44]. Determination of the graphene surface area and the dimensions of agglomerations on the graphene surface [45,46] can also be carried out with SEM. The accurate determination of individual layer thickness is, however, challenging with SEM and requires other characterisation methods, such as transmission electron microscopy [45]. The energy dispersive X-ray spectroscopy (EDS) detector provides elemental information through an X-ray spectrum and is often used to quantify the elemental

composition of the sample [47]. This can be used to identify impurities in the sample. SEM and EDX analyses were conducted in the thesis to observe the qualitative purity of the starting materials as well as produced graphene and to compare the composition and agglomerate sizes of graphene layers fabricated with different graphite samples.

3.4 Graphene as a precursor for thin film fabrication

The ultrathin 2-D structure together with its conductive and flexible character of graphene are naturally suitable properties for thin films. Graphene thin films can be produced with many methods depending on the form of the source material and the nature of the substrate. Graphene thin films have high potential as conductive components for several applications, such as flexible energy storage units for wearable electronics or roll-up displays. The use of graphene in sensors, as mentioned before, is in growing demand and could also benefit from graphene in the form of thin films. Chun *et al*. reported a method for fabricating a thin graphene film as a strain sensor component using a photolithography-patterned monolayer graphene surface on a polydimethylsiloxane (PDMS) substrate. The graphene was deposited on the PDMS surface with liquid-phase spray-coating and the product showed good stretchability [57].

Illakkiya *et al*. have used reduced GO to produce a pure graphene film. GO was selected as a starting material to avoid the issues concerning pristine graphene production. The GO was reduced with dextrose and hydrazine hydrate, followed by sonication and heating. The resulting graphene was used successfully to produce thin films onto a glass substrate with nebulised spray pyrolysis, in which the graphene dispersion was distributed into small drops by a nebuliser and sprayed with pressurised air onto a heated glass substrate to induce drying. Analyses showed the product to have similar properties to other graphene-based sensors reported earlier and the method was stated to have potential as a cost-effective and simple film fabrication method [48].

4 Experiment materials and methods

The materials, methods, instruments and process parameters used are described in the next chapters. In addition, the experiment series conducted to examine the materials and the effect of the process parameters are described.

4.1 Graphite and sodium cholate

Four different graphite samples (Table 1) were used in the experiments. Two of them were of Finnish origin, excavated from Haapamäki, and two others were of commercial origin with different particle sizes: The Finnish graphite samples, #3 and #6, have been named earlier by running numbers in the graphite treatment process. They have undergone different purification methods. The SA graphite had the largest particle size of over 150 µm and AA had the smallest, with particle size distribution under 45 µm. The particle size distribution of the Finnish samples was somewhere between the two commercial samples. The possible effect of the difference in particle size was experimented on and discussed during the thesis.

Table 1. Graphite samples used for the thesis experiments.

Graphite	Purification method	Purity ~ %
Finnish #3	NaOH + HCl	93
Finnish #6	NaOH + HCl + HF	99
Finnish #9	NaOH + HCl	N/A
Sigma-Aldrich (largest flake size, > 150 µm)	N/A	99,9
Alfa Aesar (smallest flake size, < 45 µm)	N/A	99,9

The first stages were the same for graphite #3 and #6, including sawing/crushing, froth flotation and chemical leaching with NaOH and HCl. The graphite #6 was

additionally purified with HF leaching. The graphite sample #9, which resembles the two other Finnish graphite samples, was used as reference for the determination of particle size distribution.

The sodium cholate hydrate used was produced by Acros Organics. It had been dried in an oven at ≈ 100 °C and cooled in a desiccator prior to dilution to remove the crystallised water.

4.2 Dispersion fabrication and characterisation

The liquid-phase exfoliation method used in this thesis involved shear exfoliation of graphite particles in an aqueous SC solution with a Polytron PT1200E rotor-stator mixer, maximum speed at 24 500 rpm, or a larger PT 10-35 rotor-stator mixer with an optimal exfoliation speed at 19500 rpm. The mixing speed was monitored with a Clas Ohlson standard AT-6 tachometer. The exfoliation was let to sediment for approximately 24 hours and centrifuged afterwards with a Hermle Z200A centrifuge to separate the larger impurities and unexfoliated graphite flakes from the graphene dispersions.

The centrifugation was performed in two parts: at halfway, the supernatant was transferred into a clean centrifuge tube to minimise the amount of sediment at the end of the centrifugation and to make the collecting of the supernatant easier. The supernatant was harvested afterwards for characterisation and further use.

The absorbance of the graphene dispersion was determined with a Shimadzu UV2501PC spectrophotometer. The graphene yield was calculated from the results of the UV-Vis analysis results using Lambert Beer's Law:

$$\frac{A}{l} = \varepsilon \cdot C$$

where A is the absorbance given by the UV-VIS spectrometer, l is the distance which the light travels through the dispersion, ε is the mass extinction coefficient which is 6600 ml mg^{-1} m^{-1} for graphene dispersions with high concentration and C is the mass concentration of the dispersion. The wavelength at which the absorbance was recorded was 660 nm [50].

UV-Vis spectroscopy was also used to observe the stability of the dispersion by measuring the absorbance after some days and finally after 7 days of shelf-life. The fabrication process is presented in Figure 5.

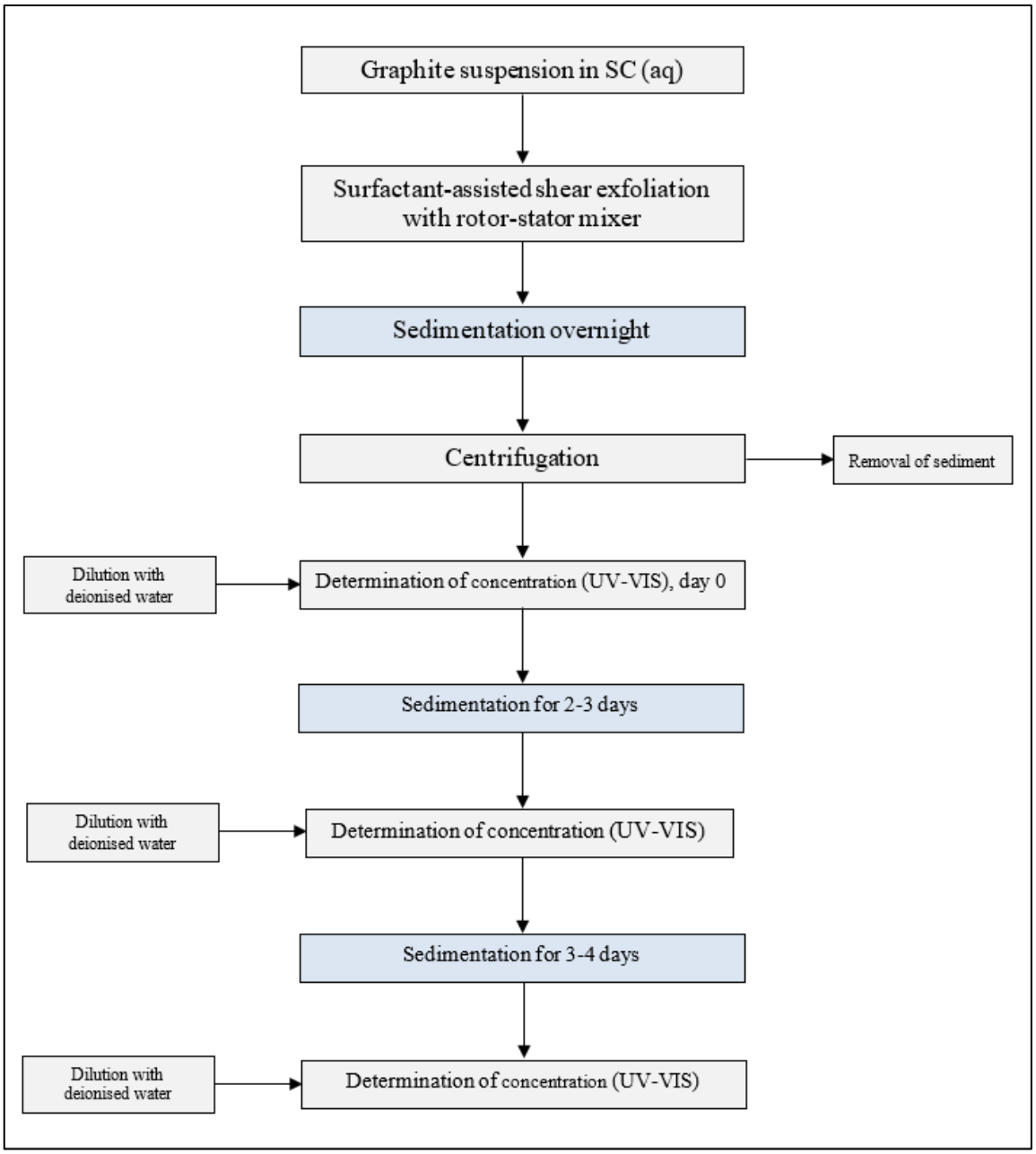

Figure 5. Overall description of the graphene fabrication process and subsequent stability follow-up.

The quality of graphene was examined with SEM and EDX analyses with a Leo 1530 Gemini scanning electron microscope. The SEM images were taken to examine the shape of the graphene flakes and the topography of the graphene

surface immobilised on the substrate. The EDX spectra gave an understanding of the elemental composition and the residual impurities of the samples. In addition, SEM images have earlier been taken from the Finnish graphite samples but not of exfoliated graphene flakes. EDX spectra of the graphene samples are also of interest since this analysis has not been performed during earlier research.

The SEM images were taken of single sample droplets dried on aluminium at room temperature. For EDX analysis, several droplets of graphene dispersions were dried on top of each other on copper plates in an oven at ≈70 °C, to obtain a thicker graphene layer to mitigate the effect of the copper plate on the EDX spectrum.

4.3 Process parameters

The standard parameters for the process were chosen based on previous research in the FennoFlakes project at Åbo Akademi. The parameters were tested and altered to empirically determine which ones affected the final concentration the most, i.e. with which values could the highest graphene yield be achieved. The standard parameters are presented in Table 2.

Table 2. Standard parameters for the shear exfoliation process.

Parameter	Standard value
$conc_{graphite}$ (mg/ml)	20
$m_{graphite}$ / sample	200 ± 0,5 mg
V_{SC} / sample (ml)	10
$conc_{SC}$ (mM)	5
t_{mixing} (min)	30
n_{mixing} (rpm)	Full (≈ 24500 rpm)
$t_{centrif}$ (min)	60
$n_{centrif}$ (rpm)	1500
RCF (G)	261

The rpm (rounds per minute) values of the centrifuge are instrument-specific and the correspondent relative centrifugal force (RCF) or G-force could be calculated.

All the rpm values used and the corresponding RCF values are presented in Table 3. The RCF value corresponding to 750 rpm was calculated with

$$RCF = 11{,}18 * r * (\frac{rpm}{1000})^2,$$

when the radius *r* was 10.38 cm. The radius was determined as the distance from the centre of the instrument into the bottom of the tube rack [49].

Table 3. Centrifugation speeds and corresponding RCF values [49].

Centrifugation speed (rpm)	RCF (G)
500	29
750	65
1500	261
2500	726
4000	1858
5000	2904
6000	4182

4.4 Experiment series

Several test series were performed to examine the effect of each parameter on the graphene yield. A detailed summary of the experiment series is presented in Appendix A. Different centrifugation speeds (500-6000 rpm) were tested together with different centrifugation times (30-120 min) to see the effect of the centrifugation parameters on the graphene yield as well as the dispersion stability. A test series with different initial surfactant concentrations (0.1-50 mM) was also performed and in order to establish the optimal concentration for the exfoliation process. Several dispersions were produced with different exfoliation durations (15-240 min) to examine how the graphene concentration changes as a function of time. The initial graphite concentration was also changed from the standard 20 mg/ml to observe the optimal concentration for a maximum yield. The highest concentration tested was 200 mg/ml. The particle size distribution of the Finnish graphite #6 was determined and compared to a similar graphite sample #9. The effect of the particle size distribution on the exfoliation process was also evaluated. The repeatability of the process was also estimated by performing identical exfoliations and by

performing error source analysis. The results of the test series were used to optimise the process parameters to achieve a maximum graphene yield with adequate dispersion stability.

4.5 Graphene yield

The graphene yield of the exfoliation as separation process is given as mass concentration. The yields are given mostly in µg/ml, as they were all fairly low. However, the low concentrations were not considered as poor results, as they are characteristic for the process. The highest graphene yields, with higher initial graphite concentrations, did not exceed 2 mg/ml.

Table 4 shows example concentrations given by each graphite sample, to show the approximate level of yield for each sample. The yields were achieved while using the standard graphite concentration. The results for #3 and #6 are average values calculated from three exfoliation replicas. The variation of the results is described in chapter 5.4, discussing the repeatability of the process.

Table 4. Example concentrations for graphene dispersions fabricated with each graphite sample in use.

Graphite	Conc. (µg/ml)
SA	23.9
#3	9.09
#6	8.13
AA	4.14

The yield varied significantly between the samples and even the Finnish graphite samples had a slight difference in concentration. They also experienced some variation between measurements and replicas fabricated at the same time, supposedly due to error sources in the process. The highest yield achieved during the experiments was as high as 1.8 mg/ml with AA graphite, while the lowest concentrations were under 4 µg/ml for the same graphite.

4.6 Thin film fabrication and initial characterisation

The graphene dispersions were tested as a starting material for thin film fabrication. The dispersion was sprayed on a clean glass plate with an airbrush. The graphene films were produced with a standard Biltema airbrush, using a heating plate for pyrolysis. As the dispersion dried on the plate the graphene particles formed a thin conductive film. Several parameters and circumstances affect the spray deposition process. These include:

- the graphene concentration of the dispersion
- spraying distance from the spray nozzle to the substrate
- duration of continuous spraying
- drying time between continuous sprays
- total spraying time, from a clean substrate to a finished film
- pre-treatment of substrate to enhance spreading, for example plasma cleaning
- no heating/heating to induce drying (i.e. spray pyrolysis)
- attachment methods for immobilising the substrate during the spraying
- pre-treatment of the sprayed dispersion (dialysis/no dialysis)

The area sprayed should, by specifications set for this thesis, be covered with graphene uniformly and preferably on a symmetrically shaped area. Since it is hard to keep the glass plate in place while spraying and pinning the plate down without covering it unsymmetrically, immobilizing the plate by using tape should be the technique with the most potential. However, if spray pyrolysis is used to shorten the drying time, the tape must tolerate high temperatures to endure the spray deposition. The pre-treatment of the sprayed dispersion also affects the outcome. In this thesis, the use of dialysis to remove excess surfactant from the dispersions was tested as a pre-treatment method for the dispersions, as the surfactant molecules can hinder the electrical conductivity of the films. The optimal product of spray deposition is a symmetrically shaped, uniform, adequately thick and electrically conductive graphene film.

The electrical resistivity of the thin graphene films produced was measured with a Fluke digital multimeter and the electrical conductivity of the films was determined as the reciprocal value of the resistivity [58], and evaluated roughly as an initial quality test of the performance level of the film.

4.7 Instruments

The exfoliation was carried out with a Polytron PT1200E rotor-stator mixer, maximum speed at 25 000 rpm, or a larger PT 10-35 rotor-stator mixer with an optimal exfoliation speed at 19500 rpm. The mixing speed was monitored with a Clas Ohlson standard AT-6 tachometer. The centrifugation was performed with a Hermle Z200A centrifuge. The UV-Vis measurements were carried out with Shimadzu UV2501PC. SEM images and EDX spectra were obtained with a Leo 1530 Gemini scanning electron microscope. The graphene films were produced with a standard Biltema airbrush, using a heating plate for pyrolysis. The initial electrical conductivity measurements were performed by measuring electrical resistivity with a Fluke digital multimeter.

5 Results and discussion

The results of the test series are compiled in this chapter and discussed according to the findings in the experiment results. The differences between the graphite samples used and the effects of the critical process parameters are presented numerically and graphically. The repeatability of the process is also discussed together with the error sources that affected the outcome and created variation between the results. The stability of the dispersions was also estimated through the results of the observation periods of each test batch.

5.1 Graphene quality and purity

The first SEM images of the graphene samples were very opaque and hard to interpret, due to the excess surfactant in the graphene dispersions which dried on the sample surface. The next SEM sample series was treated with dialysis for 7 days to remove as much excess surfactant as possible before drying in room temperature. The images taken from the dialysed samples are shown in Figure 6. The images were less opaque, and hence dialysis can be considered as a successful method for the removal of excess surfactant.

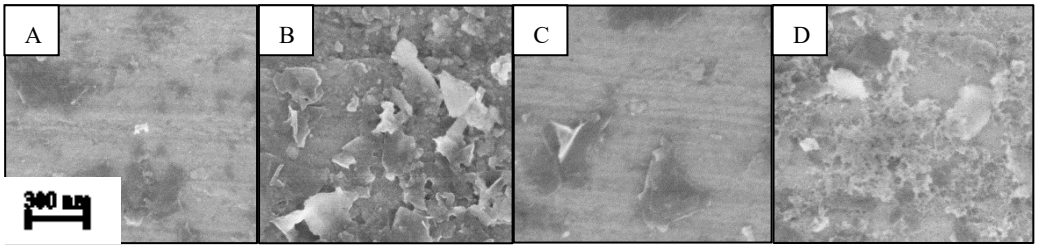

Figure 6. Set of SEM images (50 000x magnification) for the graphite samples. A. Sigma-Aldrich. B. Alfa Aesar. C. Finnish #6. D. Finnish #3.

The images in Figure 6 show the different nature of the produced graphene dispersions. The graphene dispersion fabricated with the Sigma-Aldrich (Figure 6 A) shows a very thin layer of small graphene particles on the Al-surface. The dispersion fabricated with Alfa Aesar graphite (Figure 6 B) gave an image with a

thicker layer, showing larger graphene flakes piled on each other. The graphene produced with the Finnish graphite #6 (Figure 6 C) produced a very thin layer on the Al-plate, although showing larger particles than in Figure 6 A. Figure 6 D, presenting the SEM image of graphene produced with the Finnish graphite #3, shows again a thicker layer of small particles, which are hard to distinguish from each other. Although a significant amount of the excess surfactant in the dispersions was removed with dialysis and the images taken are sharper, some surfactant molecules were most probably still attached to the graphene and make the images opaque and difficult to interpret.

The SEM images and the EDX spectra of these samples revealed the graphene layer to be too thin, as only one droplet had been dried on the Al-plate for analysis. This led to a very high Al-peak in the EDX results (Appendix B and C) which distorted the other findings in the sample. Some impurities were also detected in the samples dried on Al-plates. An additional set of EDX samples was prepared by drying multiple droplets in an oven at approximately 70 °C onto a clean Cu-plate. The EDX spectra (Appendix D and E) revealed a group of impurities which were not found earlier. Additional analyses of the untreated commercial graphite samples (Appendix F and G) and the dried SC (Appendix H) revealed some impurities but not in the same extent as the second EDX analysis. This suggests that the impurities had migrated into the samples along the fabrication process.

The quality of the graphene samples were anticipated to differ between samples, as the graphite samples used varied in particle size and purity. Yet, through SEM analysis it was discovered that the differences were not as distinct as expected. The flake shape and size varied between sample images, and a logical motivation was difficult to establish. As the process is not entirely controlled, and the graphite shears into graphene flakes of varying size and shape, the SEM images showed the resulting surfaces to be composed of numerous different flake sizes and aggregates, as well. As shown in Figure 6, the graphene samples produced from the Finnish graphite #6 was shown to have larger graphene flakes in a thinner layer than the graphene dispersion produced with #3 graphite, which showed a thicker layer of smaller particles. In addition, the excess SC makes it difficult to establish, which supposed impurities are of geological residue and which are dried SC on the graphene surface or between the graphene flakes.

The EDX analyses performed on the dried graphene samples showed that the samples had accumulated impurities during the process. It is yet to be shown which process stage is responsible for the contaminant migration, or if the EDX is reliable as a method on its own and the result should be confirmed with another suitable analytical method. The effects of the impurities on the dispersion and thin film quality are also still unknown.

5.2 Dispersion stability

As the graphene sheared of the graphite particles vary in size and shape, the sedimentation rate of the colloidal particles is hard to predict by calculation. The effect of the parameters on the dispersion stability during the first week was studied to potentially minimise the sedimentation of particles during shelf-life while still maintaining the yield as high as possible. The effect of the centrifugation speed on the dispersion stability is presented in Figure 7. As it can be seen, the concentration decreases and the dispersion becomes more stable with increasing centrifugation speed. The centrifugation time for these samples was kept at the standard 60 minutes.

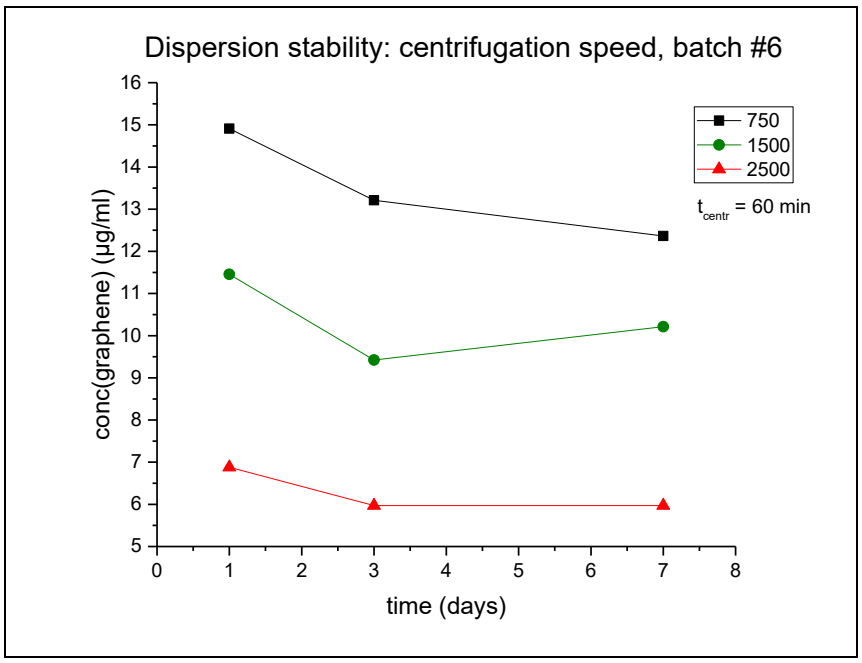

Figure 7. The effect of centrifugation speed on the stability of the dispersions. The increase shown on the 1500-rpm curve is caused by sedimentation rise during pipetting.

Figure 7 shows that the most stable dispersion is the one centrifuged with a speed of 2500 rpm and that the 750-rpm speed is not sufficient to produce s stable dispersion, as the concentration continues to decrease even after 7 days of shelf-life. The increase of concentration seen in the 1500-rpm curve is a result of an experimental error, caused by sedimentation rise during pipetting. This occurs easily for the last measurement points, since the sample volume is extremely low and the dispersion surface is very close to the sedimentation on the bottom of the vial. This distorts the final result and the final result cannot be determined without eliminating the measurement point.

Figure 8 shows the effect of centrifugation time on the dispersion stability. The increasing centrifugation time decreases the final concentration. Regardless of the increase in concentration in the 60-minute series (due to an experimental error), the increase in centrifugation time seems to make the dispersions more stable.

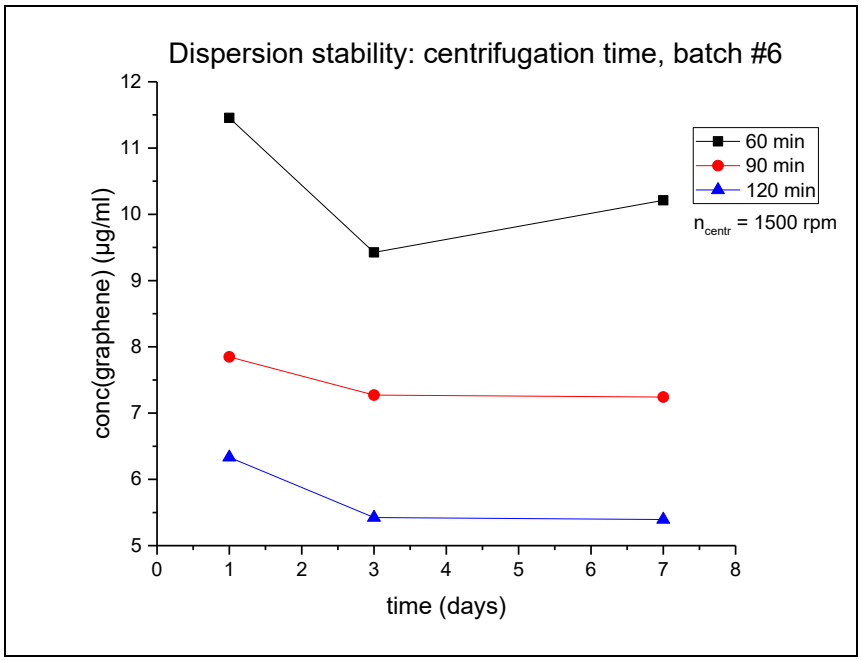

Figure 8. The effect of centrifugation time on the stability of the dispersions.

In Figure 9, the stability of all four samples treated with standard parameters are compared. As shown, the final concentration of the graphene dispersion varies considerably depending on the used graphite sample. Ignoring the minor concentration increase between the last time points, which may be caused by

pipetting issues due to the small sample volume, the Finnish graphite samples seem fairly stable during the first week.

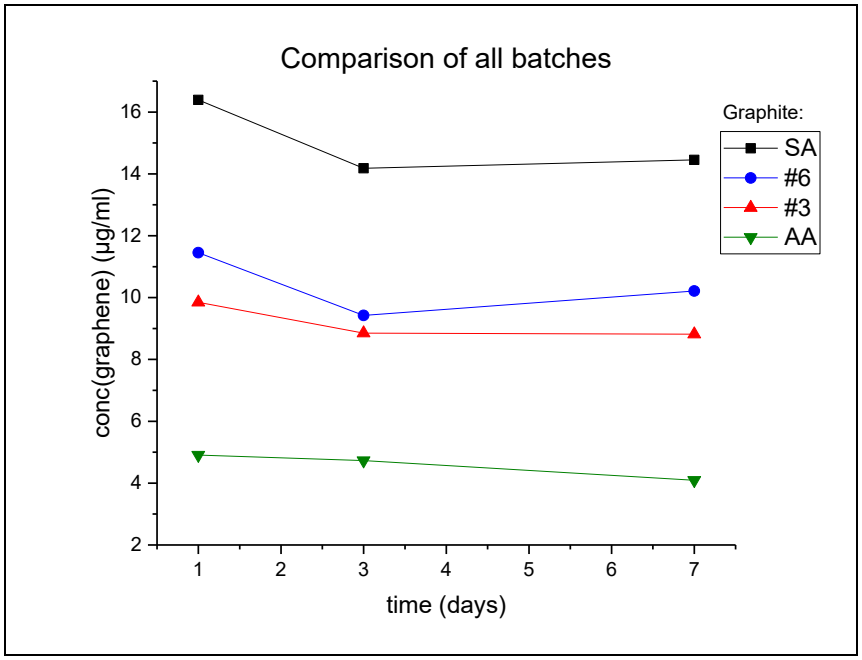

Figure 9. A comparison of stability results obtained with different graphites.

One of the key factors affecting the stability of the dispersion is the particle size of the source material. Experiments showed that a relatively higher yield could be achieved with the Sigma-Aldrich graphite, which had the largest particle size. However, the larger the particle size, the more instable the final dispersion was as a function of time. On the other hand, the Alfa Aesar with the smallest particle size should produce the most stable dispersions, but this assumption does not always comply, and these dispersions can show as much instability as the other samples. The Finnish graphite samples had a particle size between the two commercial samples, and so is the yield and relative stability of the dispersions. The effect of the particle size was discussed further in chapter 5.3.5.

It was also established that both the centrifugation speed and time have an effect on the stability of the dispersions. An increase in either parameter, especially centrifugation speed, led to more stable dispersions as a function of time due to lower final graphene concentration. The higher centrifugation speed made the sedimentation of larger particles more effective during centrifugation, thus lowering the amount of sedimentation during the observation period. The optimal

stability was achieved with a centrifugal speed of 1500 and 2500 rpm, from which the lower speed was chosen as the optimal parameter, as it promotes slightly higher yield.

As was mentioned, the stability of the dispersions does not only depend on the parameters of the process, but also the storing conditions after the exfoliation. The dispersions stored in glass vials are highly sensitive to any kind of shaking, tremor or tilting. The vials have to be stored in a stable environment and treated with care and without sudden movements when taking samples for stability measurements. The pipetting must be carried out carefully, as the sediment rises easily from the bottom of the vial. Some graphene platelets may also rise to the supernatant surface, and pipetting these should also be avoided. The small amount of the liquid in the sample often makes this challenging, and changes the stability observed during the waiting period. Larger fabrication volumes may make the process more favourable, considering shelf-life and pipetting of samples.

5.3 Critical parameters

The exfoliation and graphene harvesting process studied during the thesis experiments consists of numerous parameters which affect the final graphene yield in the aqueous dispersion. Through empirical research, other parameters were observed to have a critical effect on the yield, as well. In the next chapters, these parameters and their effects on the process are described individually according to the experimental results.

5.3.1 Centrifugation speed and time

During earlier research within the FennoFlakes project, several parameters have been studied and discussed concerning their effect on the outcome of the exfoliation process. However, centrifugation speed and time had not yet been looked into. It has been assumed that a higher centrifugation speed decreases graphene yield, yet produces somewhat more stable dispersions, as the larger and heavier particles

sediment to the bottom of the tube. The effect of the altered centrifugation speed as a function of the centrifugation time can be seen in Figure 10. The Finnish graphite batch #6 was used in the experiments. It can be concluded that both the increasing centrifugation speed as well as duration have a decreasing effect on the graphene yield.

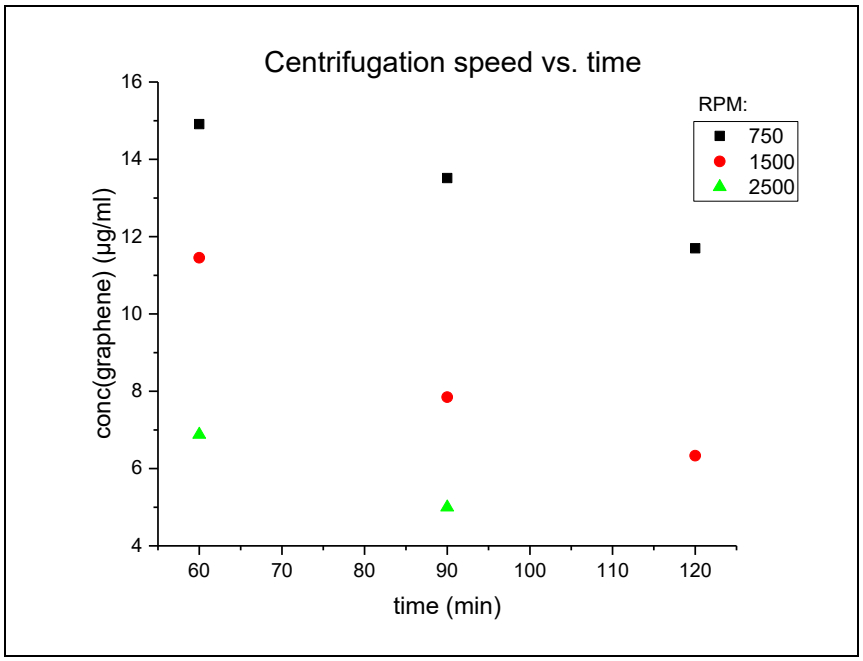

Figure 10. The effect of centrifugation speed on the graphene yields a function of time. The third measurement point for 2500 rpm series is missing due to sample insufficiency.

5.3.2 The initial surfactant concentration

Earlier studies had shown that the highest graphene yield can be achieved with a surfactant concentration of 1-10 mM [51]. The critical micelle concentration (c.m.c.) of sodium cholate is known to be 9-14 mM [52]. The c.m.c. has been reported as the optimal graphite dispersion concentration for some surfactants, but SC does not follow this mechanism [53,56]. A 5 mM surfactant concentration was used as a standard parameter, since it has continuously given optimal results. The SC used during earlier research differs from the one used for the thesis, and this is one of the reasons why the surface tension of the aqueous surfactant solution was

measured in different concentrations, thus determining the c.m.c. of the SC used. In addition, exfoliation test series were performed with the same concentrations used for the surface tension determination and the resulting trends were compared to see the effect of the concentration on the yield.

The results of the surface tension determination and the SC exfoliation series are shown in Table 5. The results of the exfoliation test series are shown together with the ln(surface tension) curve in Figure 11. The 6 mM result has been eliminated from the graph as an outlier.

Table 5. The measurement points and results of the surfactant concentration experiments.

Conc(SC) (mM)	Surface tension (Nm m^{-1})	ln(surface tension)	Graphene conc. (µg/ml)
0.1	62.7	4.14	6.76
1	53.9	3.99	5.73
5	52.2	3.96	8.42
6	40.7	3.71	8.36
7	50.2	3.92	7.82
8	49.0	3.89	7.24
9	49.1	3.89	8.73
10	49.7	3.91	8.46
20	48.9	3.89	7.36
50	48.1	3.87	3.97

The c.m.c. region can be determined from the curve as the region just before the curve slope starts to even out [54], which is between 5 and 10 mM. The yield reaches the maximum within the SC concentration range of 5 and 10 mM. The variation in the graphene concentration at the c.m.c. area may also be caused by error sources in the process, such as pipetting or an instrumental error. The 5 mM concentration can this way be stated to be a suitable parameter for the process, when aiming for an optimal graphene yield.

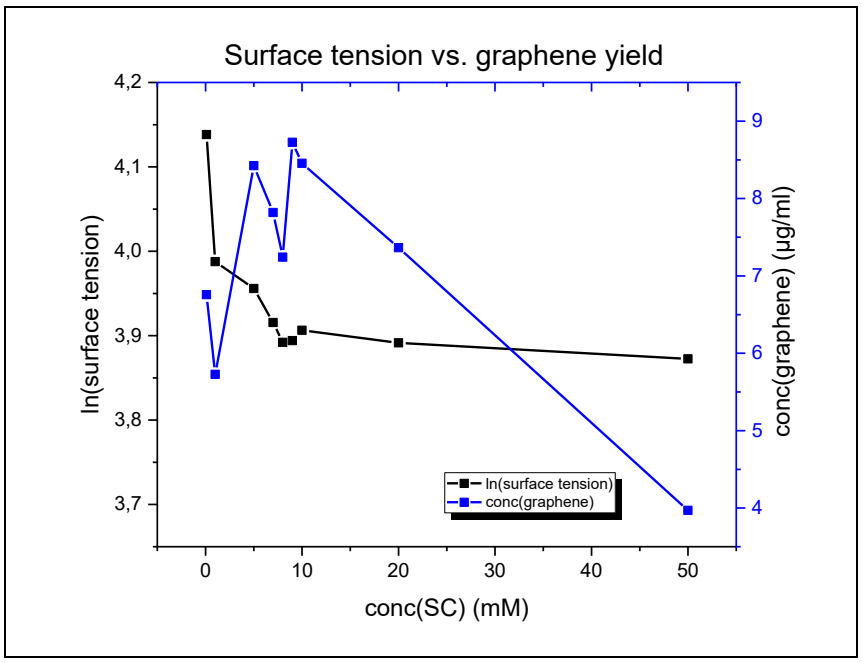

Figure 11. The results of the surface tension measurement plotted together with the surfactant concentration series results as a function of surfactant concentration.

5.3.3 Exfoliation time

The shear exfoliation process is strongly dependent on the duration of the exfoliation. The logical assumption is that as the exfoliation time is prolonged, the yield should increase as well. To test the linearity of this phenomenon, several exfoliation experiments were performed with different exfoliation durations. The graphene yield was expected to increase as a function of exfoliation time, yet the dispersions obtained may be less stable. In addition, extremely long exfoliation times make the dispersion more difficult to handle, e.g. to transfer the dispersion from one vessel to another, as the dispersion becomes thicker due to a longer mixing time and a consequent increase in foaming.

The exfoliation results are displayed in Table 6 and graphically as a function of time with linear fitting in Figure 12. As displayed, the final graphene concentration increases linearly as a function of time, with a $R^2 = 0.99754$.

Table 6. The parameters and results of the exfoliation time series.

Sample	Mixing time min	Mixing speed	Conc. day 1 µg/ml	Conc. day 2 µg/ml	Conc. day 7 µg/ml
#6 1	15	Full	4.97	4.67	4.12
#6 *	30	Full	8.42	7.70	7.00
#6 2	45	Full	12.3	11.7	9.70
#6 3	60	Full	14.4	13.2	12.1
#6 4	90	Full	20.2	18.7	17.8
#6 5	120	Full	27.5	26.4	23.6
#6 6	180	Full	40.6	37.3	36.8
#6 7	240	Full	50.8	46.6	44.9

* determined earlier, an average result of three replicas

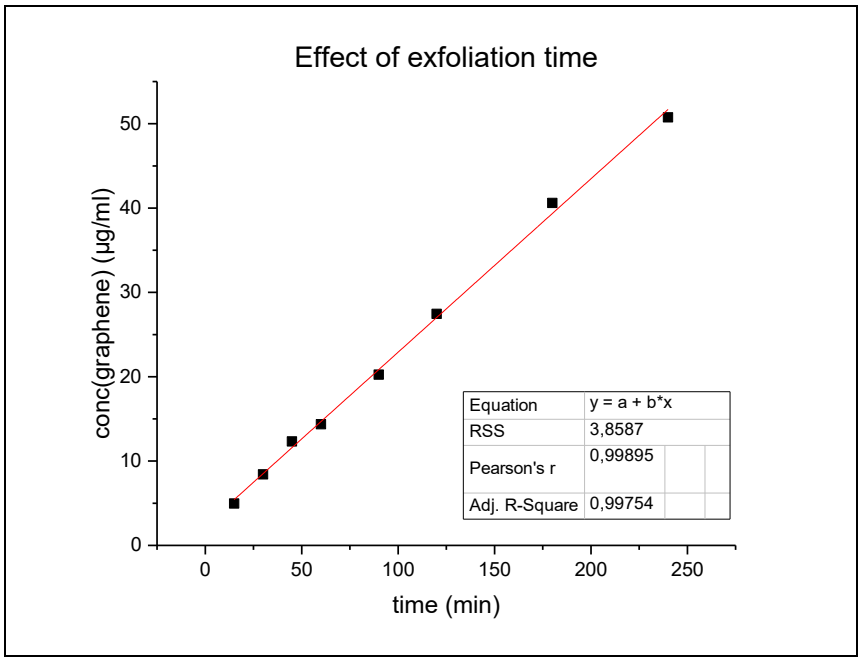

Figure 12. The results of the exfoliation time series with linear fitting.

5.3.4 The rotor diameter and the initial graphite concentration

The effect of the initial graphite concentration has been investigated during earlier studies, but similar tests were repeated in the thesis, as the graphene yield had not achieved the same level as earlier in the project. The exfoliations were performed on two different mixers: the smaller PT1200E with PT DA 07 mixer end (d_{rotor} = 4.85 mm, shear rate $\dot{\gamma} = 51600\ s^{-1}$ at the maximum exfoliation speed) and the PT 10-35, with PTA 20 S mixer end, which is larger in rotor diameter (d_{rotor} = 15.15 mm, shear rate $\dot{\gamma} = 68700\ s^{-1}$ at an exfoliation speed of 19500 rpm). The difference in rotor diameter leads to a significant difference in maximum shear rate for the mixers [55]. The difference in yield for the two mixers is of interest as one aim of the thesis was the maximum graphene yield of the process.

The initial concentrations ranged from 50-200 mg/ml and an earlier exfoliation with the standard graphite concentration was included into the results for the smaller mixer. Maximum exfoliation speed was used in exfoliation with the smaller mixer. 19500 rpm was chosen as exfoliation speed for the larger mixer according to earlier research [55]. The results are shown in Figure 13. The comparison of the two curves shows that higher yields can be achieved with the larger mixer due to the higher shear rate. Some linearity can be observed from the trends of the curves. These could be used as standard curves to approximate a yield for an upcoming exfoliation process.

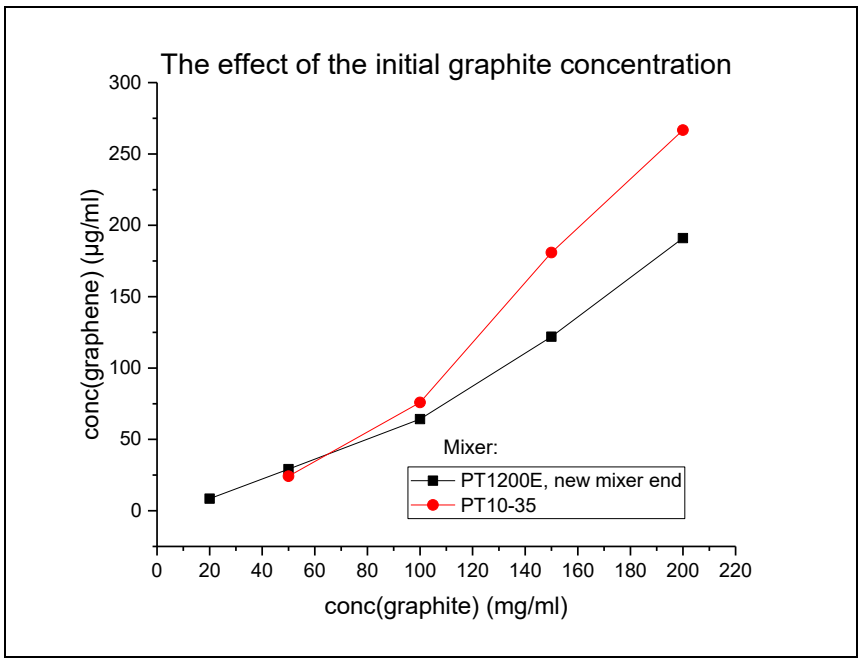

Figure 13. The results of the graphite concentration series performed with two mixers. The smaller mixer results also display a measurement point for an earlier experiment with a 20 mg/ml graphite concentration, as reference.

The effect of the initial graphite concentration was similar to the exfoliation time: the higher the value, the higher the graphene yield. Yet, the stability of the dispersion decreased as a function of time at higher graphene concentrations. The loss of source material also increased, since the efficiency of the process was constant, regardless of the amount of the graphite. The dispersion was, additionally, more challenging to harvest with the increased amount of dry matter in the suspension.

5.3.5 The graphite particle size

The effect of the graphite particle size on graphene yield was investigated in the thesis as an important parameter. In Figure 9 (ch. 5.2), the dispersion stability of all the samples were compared. In addition to the observed stability of all samples, the final concentration achieved seemed to be in relation to the particle of the initial graphite used: as SA has the largest particle size (> 150 µm) and its final graphene concentration is the highest and the dispersions are less stable compared to the other samples. The Finnish graphite samples both showed fairly similar results, with a slight difference. The higher yield was achieved with the #6 graphite that had a

higher purity level. The Alfa Aesar graphite has the smallest flake size (< 45 μm) and gave the lowest graphene yields. It was of interest to perform a test series with graphene samples of varying particle size to see how a narrower particle size distribution affects the graphene yield of the Finnish graphite samples.

The particle size distribution was determined by sieving a weighed graphite #6 sample at the laboratory of geology at Åbo Akademi University. Every sieve lets through particles with a specific size and the larger ones remain in the sieve. The fractions for each sieve are listed in Table 7. The first particle size distribution experiment was performed on approximately 40 g of graphite #9, which is comparable to the two Finnish graphite samples in use in original source and particle size. Afterwards, the determination was repeated with 6 g of the #6 graphite. The mass of graphite needed for the exfoliation was calculated for one sample as well as for 3 replicas. The calculations were based on the particle size distribution of the graphite sample #9 and the demand of the exfoliation process.

Considering the particle size distribution of the samples, it can be established that the particle size distribution of graphite #6 is close to the size distribution of Finnish graphite #9 (Table 7 and Figure 14).

Table 7. The calculations performed according to the fraction distribution of graphite #9 and the results of the fraction sieving of #6.

d (μm)	m-% #9	required for 1 sample (à 0.2 g)	required for 3 samples (à 0.6 g)	weighed fraction mass #6 (g)	m-% #6
45-:	2.8	7.14	21.43	0.18	3.4
45-63:	**12.2**	**1.64**	**4.92**	**0.95**	**17.8**
63-125:	**35.1**	**0.57**	**1.71**	**2.05**	**38.5**
125-150:	**30.8**	**0.65**	**1.95**	**1.21**	**22.7**
150-250:	**14.6**	**1.37**	**4.11**	**0.77**	**14.4**
250+:	4.0	5.00	15.00	0.17	3.2

As the four relatively largest fractions are of highest interest, 6 g of #6 graphite was weighed and sieved to separate the individual fractions from each other. This amount was estimated to be sufficient for three samples of the four largest fractions. As seen in Table 7, the fraction masses were large enough to give three samples of the four largest fractions.

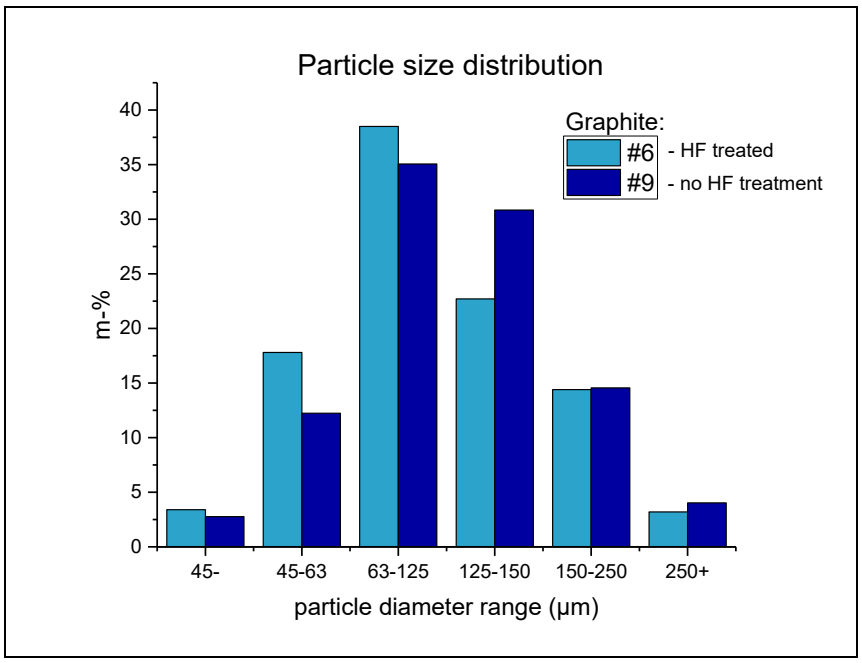

Figure 14. Comparison of the particle size distributions of graphites #6 and #9.

It can be seen that the particle size distributions of these two graphite samples are relatively similar, with some exceptions in three fractions. The #9 sample had not been purified with HF, which may break down the particles slightly and cause a difference in particle size distribution. However, the difference could also be caused by the difference in the amount of the sample: the graphite # 9 was sieved as a whole with a mass of 40 g since it was not used for any other experiments, but only 6 g was used from #6 due to the future need of the graphite.

Exfoliations were performed on the weighed samples and the results are shown in Table 8 and Figure 15.

Table 8. The results of the particle size distribution series.

Particle diameter (µm)	Conc(graphene) (µg/ml)	Average conc. (µg/ml	SD
45-63	9.64	9.03	1.05
	9.64		
	7.82		
63-125	16.9	15.3	1.42
	14.2		
	14.8		
125-150	19.0	17.7	1.32
	17.7		
	16.3		
150-250	10.9	11.7	6.92
	23.6*		
	12.6		

* = outlier

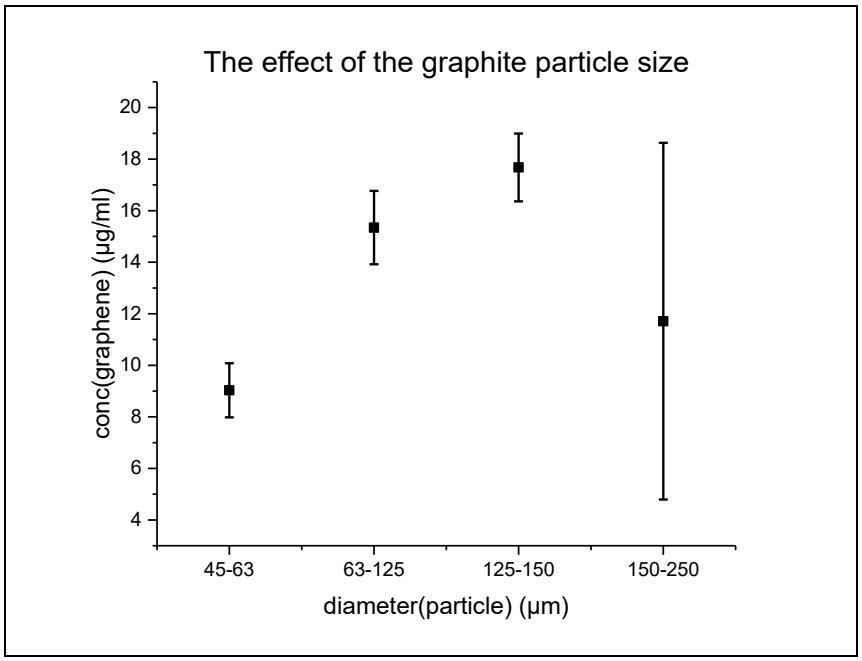

Figure 15. The effect of the graphite particle size on the final graphene yield. The error bars in the graph represent standard deviation.

A large deviation can be seen in the results of the 150-250 µm fraction in Figure 15. One of the results (Table 8) deviates significantly from two other measured results. Oddly, the evident outlier would on its own set a linear dependence on the yield as a function of the particle diameter, yet the two other results resembling each

other are at least two times smaller than the third result. This may be caused by the larger range in particle size in this fraction, which may enable the shearing of the graphite in varying manners. However, the deviation does not increase as a function of particle size but is quite the same for all other fractions. Regardless of this, the yield seems to increase as a function of the particle diameter for the other three fractions.

5.4 Repeatability of the process – error sources

A process with several stages and parameters has as many sources of error. Pipetting of liquids as well as other means of transferring solids, liquids and suspensions from one container to the other increases the probability for irregularities in the results. A full-length error analysis is time-demanding and hard to carry out to such a multi-stage process. The overall variation in the process was estimated by a series of repeatability tests, performed with two graphite samples and two centrifugation speeds. The 500-rpm speed was chosen as a minimum speed, which was not used during the process, but is so low that it might cause significant variation in the final graphene yield. The Finnish graphite samples #3 and #6 were both used, and the results are compared in Figure 16. Each measurement point in the graph is an average of three determinations and the error bars represent standard deviation.
The difference caused by the centrifugation speed on the yield is evident and has some effect on the amount of variation for each measurement point. Some of the measurements were carried out on different days, which can also create variation between the results for each series. The overall behaviour of the dispersion is fairly similar and does not show any surprising outliers or deviations.

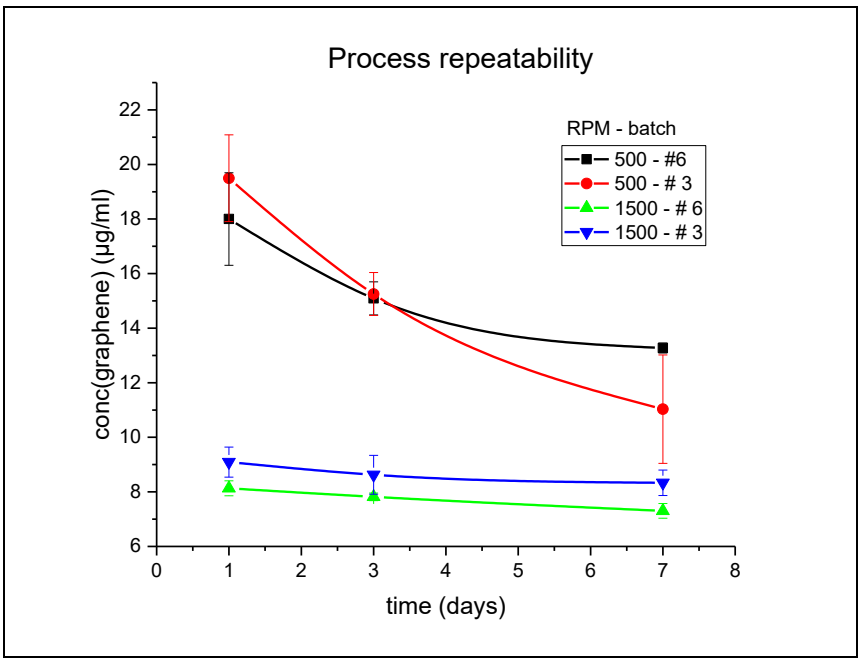

Figure 16. Process repeatability: graphene yield as a function of time, comparison over two centrifugation speeds.

5.5 The optimal processing parameters

The processing parameters, which were chosen for the process at the beginning of the thesis, were optimised through empirical studies to achieve the highest possible graphene yield while keeping the process as economical as possible. The resulting parameters are shown in Table 9.

Table 9. The essential parameters of the process and the chosen standard values together with the optimal values.

Parameter	Standard value	Optimised value
$conc_{graphite}$ (mg/ml)	20	200
$m_{graphite}$ / sample	200 ± 0,5 mg	2000 ± 0,5 mg
V_{SC} / sample (ml)	10	10
$conc_{SC}$ (mM)	5	5
t_{mixing} (min)	30	120
$n_{exfoliation}$ (rpm)	≈ 23000	≈ 23000
$n_{centrifugation}$ (rpm)	1500	1500
$t_{centrifugation}$ (min)	60	30+30

In order to achieve a maximum graphene concentration, the optimal initial graphite concentration was found to be 200 mg/ml. As the yield was linearly dependent on the amount of the source material, a further increase in the initial graphite concentration would naturally increase the yield. Further increase was not investigated, as the source material is limited by amount and the concentration achieved was high enough for film fabrication by spray deposition. To achieve this concentration, the mass of graphene was increased to 10-fold of the original amount while the volume of the aqueous surfactant was kept constant. An increase in volume would have required a further increase in graphite mass to maintain the optimal concentration. Decreasing the volume would have led to a deficiency in sample amount, considering the spraying of the films.

The surfactant concentration was kept at the optimal 5 mM, since a decrease in the concentration led to a dramatic decrease in yield when using the optimal graphite concentration. Although there is excess surfactant to be found in the final dispersion, the decreasing amount of the SC during exfoliation leads to poorer dispersion and reaggregation if the initial concentration is lowered and the SC-graphite ratio changes. The optimal mixing time was increased to 120 minutes, as it was the shortest time which produced adequately high graphene concentrations for successful film fabrication. A further increase might still increase the yield, but makes the process more time-demanding, uneconomical and difficult for the mixer to endure. The exfoliation speed was maintained at the highest value attainable (≈ 23000 rpm), since a decrease in the exfoliation speed would only lead to an unnecessary decrease in yield. Centrifugation speed, which was supposedly one of the most critical parameters, was kept at 1500 rpm. An increase in speed led to more stable dispersions, yet lowered the yield significantly. A decrease in speed gave dispersions with poorer repeatability. Centrifugation time was maintained at 60 minutes for similar reasons as centrifugation speed.

5.6 The parameters and results of the thin film fabrication

The first three film fabrication experiments were carried out without heating of the substrate. The graphene dispersions with the highest graphene concentrations were chosen for the experiments with glass substrates to produce a thick film as fast as possible. Subsequent experiments were performed on a heating plate with temperature at ≈ 200 °C to shorten the drying time. All film fabrication tests were carried out with dispersions exfoliated from Alfa Aesar graphite.
The results of the most successful experiments are displayed in Table 10.

Table 10. Summary of the film fabrication experiments with the examined parameters and the outcome of each experiment. If several dispersions were used and compared in the test, the concentrations of each dispersion are mentioned.

Test nr.	$conc_{graphene}$ (mg/ml)	Spraying distance (cm)	$t_{spray\ pulse}$ (s)	$t_{drying\ time}$ (s)	t_{total} (min)	Plasma cleaning (x/-)	Heating (x/-)	Attachment method	Result
1	1.3	5	1	20	25	x	-	Double-sided tape	Very thin
2	1.3	7-10	1	20	25	x	-	Double-sided tape	Thin, with very weak conductivity
3	1.8	10	1	20	30	x	-	Double-sided tape	Thin, with weak conductivity
4	1.8	10	3	1	6	x	x	Pinning down from one corner	Thick, yet less uniform, unsymmetrical
5	1.1	10	3	1	6	x	x	Immobilisation from four sides	Uneven result
6	0.5	10	3	1	9	x	x	Regular tape	Failed
7	0.5 /1.1	10	3	1	8	-	x	Kapton tape	Thick, yet unevenly distributed, no conductivity
8	0.4/0.7/0.8	10	10	1	25	-	x	Kapton tape	Thick, transparent, conductivity

Using double-sided tape left an additional layer of air beneath the glass plate, which increased the drying time of the dispersion, resulting in droplet formation if the spraying was performed at equal speed as during other experiments. When pinning the glass plate down from one corner, the resulting area of the thin film was

unsymmetrical by shape. Immobilising the plate without covering it was challenging, as the thin glass plate kept moving despite the barriers surrounding it during spraying. Taping the plate down from four sides was also promising, but the regular tape did not tolerate heating and melted after ≈ 9 minutes of spraying. When the tape was removed, the glass plate broke. Kapton tape showed no signs of damage due to heating and was fairly easy to remove after spraying.

The conductivity of the films was determined preliminarily by measuring the electrical resistivity of the films with a Fluke digital multimeter. The resistance was only measured from films which visually seemed thick enough. As the conductance is the reciprocal of resistivity, the conductance is evaluated to increase with decreasing resistivity values measured. The highest value for resistivity measured was with the film from experiment 3. The resistance of the film (distance ≈ 1 cm) was at the range of ≈ 100 kΩ which is still relatively high, yet promising. The films from experiment 7 were also exposed to IR incineration to eliminate the excess SC in the films and consequently increase the conductivity of the film. The incineration was successful, as the films showed very low or no conductivity before the incineration. An excess amount of surfactant may weaken the conductivity of the film, as sodium cholate is not electrically conductive. Although the incineration increases the conductivity to some extent, the increase is not sufficient. In addition, there is a risk of breakage as the glass plate is heated and cooled repeatedly during the incineration. Dialysis is another method with which some of the excess surfactant can be removed from the dispersion. After treating some dispersions of the experiment 8 with dialysis before spraying to remove the excess surfactant in the dispersion, the films gave promisingly low values of resistivity. The lowest resistivity values obtained were ≈ 10 kΩ with the third set of films, which suggests a conductance of ≈ 0.1 mS. The increase in conductivity implies that the conductivity may be high enough for the film to be tested as an electrically conductive component. Figure 17 shows some of the most successful films fabricated in the thesis.

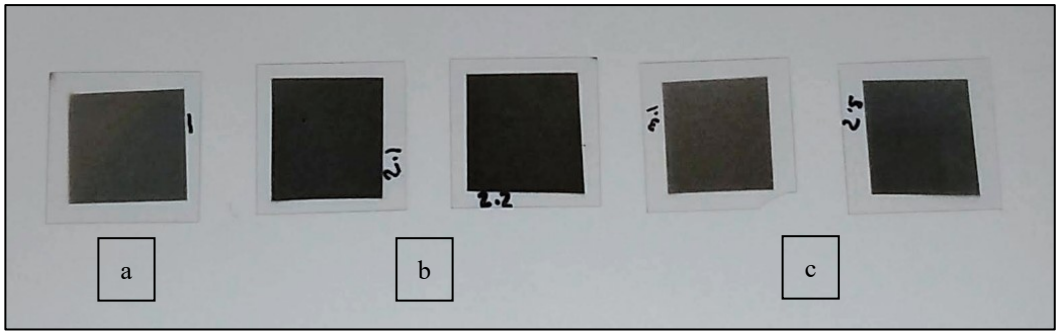

Figure 17. Graphene films produced with pyrolysis-aided spray deposition a. Graphite exfoliated with smaller mixer PT1200E, t = 2 h, and dialysed after centrifugation. b. 2 films: Graphite exfoliated with larger mixer PT10-35, t = 2 h. No dialysis. C. 2 films: Graphite exfoliated with larger mixer PT10-35, t = 2 h. Treated with dialysis after centrifugation. The films were sprayed one at a time.

The films fabricated showed increasing uniformity with an increase in spraying distance and a decrease in droplet size. Although the films seemed too thin to give adequate values of electrical conductivity, the thickness of the films improved with increasing graphene concentration. Films with a concentration of nearly 2 mg/ml showed weak conductivity, while films fabricated with dispersion concentrations of 1 mg/ml or lower showed no conductivity. This was concluded to be caused by the excess SC in the dispersion which serves as an insulator between the graphene particles. The incineration of the films with IR was not effective enough to incinerate the SC on the graphene film surface to promote conductivity. Sufficient decrease in resistance was achieved for dispersions with a concentration under 1 mg/ml when the dispersions were treated with a 24-hour dialysis before spray deposition. Heating the glass plate during the spraying shortened the spraying time significantly by speeding up the drying of the sprayed dispersion. The resistance levels measured suggest that the films fabricated with this methodology could be used in further research, investigating their potential as conductive components.

5.7 Challenges

Some challenges were discovered during the thesis while others are yet to be addressed. One major challenge was the scalability of the process. As the volumes produced by this particular method are quite small, the use of one produced sample is fairly limited to 1-2 small graphene films. As there is much variation in the

outcome of each graphene sample produced, it is difficult to produce samples with a high level of repeatability. The relative loss of source material is still quite high, staring with 0.2-2 grams of graphite and producing approximately 8 mg of graphene at highest. Scaling up the process would require increasing amounts of graphite, while the access to high-quality natural graphite is still limited.

Other practical issues include the issues noted in suspension transfer from one vessel to another. As the graphite-SC suspension is thick due to foaming, it is difficult to remove from one vessel in its entirety without leaving an amount of it into the first vessel. Another similar issue is the variation when changing the centrifuge tube after 30 minutes of centrifugation. It is fairly difficult to control the amount of sediment that follows the supernatant into the new tube, creating variation into the final yield and stability. In addition, the potential substrates for the film deposition are scarce due to the need of heating to promote a shorter drying time and the IR incineration to eliminate excess surfactant. And yet, the aqueous character of the medium itself causes spreadability, evaporation and adhesion issues and thus limits the choice of optimal film deposition techniques to spraying. On the other hand, spray deposition is a simple process in itself and a relatively fast way to produce conducting films if the challenges of the method are tackled.

6 Conclusions

The aim of the thesis was to determine the optimal parameters for the shear exfoliation process and to determine whether the Finnish graphite samples can be used for applications in a similar way as the commercial samples. The Finnish graphite shows potential as it behaves in a similar manner as the commercial samples. Despite the variation in results caused by the error sources of the process, the commercial graphite has shown no superior potential over the Finnish graphite samples. This means that the Finnish graphite could be used in similar applications as the commercial samples, if the challenges in the process are addressed with further research. The two Finnish graphite samples did show a difference in yield, but it cannot be stated to be a result of the purity difference.

According to the results of these experiments, there are four critical parameters which affect the final yield the most. One of these is the centrifugation speed, which when increased gives more stable dispersions with decreasing concentration. The 1500-rpm centrifugation speed was shown to give dispersion with an acceptable stability level, and the value was left unchanged. Collecting the dispersion is one of the most crucial error sources in the process, as the amount of the sediment rise during the collecting of the supernatant is hard to control.

Another critical parameter is the initial graphite concentration. The yield was shown to be linearly dependent on this parameter, and the highest yields were achieved by increasing the standard value to 10-fold. However, the graphite is not advised to be increased further, as the loss of source material is already significant in the proportions. If the yield needs to be increased further, should the other parameters be looked into and the optimal value for the graphite concentration should rather be considered as the maximal value.

The third critical parameter is the exfoliation time, which follows the same pattern as the graphite concentration. The highest yields were obtained with an exfoliation time of 240 minutes, yet the optimal value was set to 120 minutes instead, as it was sufficient to produce graphene dispersions for successful film fabrication. While there was no increasing loss of material due to the increase in exfoliation time, the

process becomes time- and energy-consuming. As the volumes produced are still quite small, a prolonged fabrication time makes the process unfavourable. Although the highest yields have been achieved with the 240-minute exfoliation, the best signs of conductivity were reached with a 120-minute exfoliation combined with a 24-hour dialysis after the centrifugation. Although this makes the process time even longer, it mitigates the need for a long exfoliation time and perhaps even allows the decrease of the initial graphite concentration.

The fourth critical parameter is the graphite particle size. This was shown through the experiments conducted with four samples with significantly different particle sizes and even by fraction distribution within one sample. The highest yields within standard parameter values were achieved with the Sigma-Aldrich graphite, which had the largest flake size. The particle size distribution experiment showed that the highest yield, with the least deviation between replicas, was obtained with the 125-150 µm particle fraction. This is also one of the dominating fractions for the Finnish graphite sample #6. The effect of the particle size on the resulting graphene films is yet to be studied.

The difference in purity did not show any dramatic effects on the final yield. The two Finnish samples, which experienced different purification methods, show relatively similar results. There were minor differences in yields between the samples, but it could be caused by the error sources in the process and could not be traced back to the difference in purity. This suggests that some of the purification steps could be eliminated in the future to avoid overprocessing of the source material.

One limiting factor concerning the use of the graphene dispersions is the excess surfactant, which is crucial for the exfoliation process but may inhibit the electron mobility in the fabricated thin graphene film. The dialysis of the dispersions before spray deposition was shown to decrease the resistance measured in the films fabricated during the initial tests. This means that this process may be used to produce films to be tested as a conductive component in e.g. an environmental sensor.

During the thesis, the process parameters regarded as essential were examined and an optimisation was successfully carried out as a result of the numerous experiments conducted for each parameter. Several important aspects were learned about the

controllability and the critical points of the production process. The Finnish graphite samples were compared with the commercial samples and the differences between them were pointed out, of which relative purity did not seem to be a crucial factor. The impurities found from the graphene dispersions may need further examination to establish if they need to be taken into account or if they can be neglected as unessential to the process. Some development points were established for future investigation, on which new research may take ground on. Regardless of the error sources and challenges of the process, thin films indicating a potential for functional use were the main successful result of this thesis.

References

[1] Soldano, C., Mahmood, A., Dujardin, E. Production, properties and potential of graphene. *Carbon* **2010**, 48, 2127-2150.

[2] Simandl, G. J., Paradis, S., Akam, C. Graphite deposit types, their origin, and economic significance. Symposium on critical and strategic materials. *British Columbia Geological Survey Paper* **2015-3**, 163-171.

[3] Ahtola, T., Kuusela, J. Esiselvitys Suomen grafiittipotentiaalista. Geological Survey of Finland **2015**, 1-14.

[4] Geim, A. K. Graphene – status and prospects. *Science* **2009**, 324, 1530-1534.

[5] Novoselov, K. S., Geim, A. K., Morozov, S. V., Jiang, D., Zhang, Y., Dubonos, Grigorieva, I. V., Firsov, A. A. Electric Field Effect in Atomically Thin Carbon Films. *Science* **2004**, 306, 666-669.

[6] Novoselov, K. S, Fal'ko, V. I., Colombo, L., Gellert, P. R., Schwab, M. G., Kim, K. A Roadmap for Graphene. *Nature* **2012,** 490, 192-200.

[7] Singh, V., Joung, D., Zhai, Lei, Das, S., Khondaker, S. I., Seal, S. Graphene based materials: Past, present and future. *Progress in Materials Science* **2011**, 56, 1178-1271.

[8] Yang, W., Ratinac, K. R., Ringer, S. P., Thordarson, P., Goodin, J. J., Braet, F. Carbon Nanomaterials in Biosensors: Should You Use Nanotubes or Graphene? *Angewandte Chemie International Edition* **2010**, 49, 2114-2138.

[9] Lee, C., Wei, X., Kysar, J., Hone, J. Measurement of the elastic properties and intrinsic strength of monolayer graphene. *Science* **2008** 5887, 385-388.

[10] Yang, Y., Han, C., Jiang, B., Iocozzia, J., He, C., Shi, D., Jiang, T., Lin, Z. Graphene-based materials with tailored nanostructures for energy conversion and storage. *Mater Sci Eng R* **2016**, 102, 1-72.

[11] Yoon, H. J., Jun, D. H., Yang, J. H., Zhou, Z., Yang, S. S., Cheng, M. M-C. Carbon dioxide gas sensor using a graphene sheet. *Sens Actuators B Chem* **2011**, 157, 310-313.

[12] Mohan, V. B., Lau, K-t., Hui, D., Bhattacharyya, D. Graphene-based materials and their composites: A review on production, applications and product limitations. *Composites Part B* **2018**, 142, 200-220.

[13] Mandal, S. K.*: Steel Metallurgy - Properties, Specifications, and Applications*. McGraw Education (India) Private Limited, **2014**.

[14] Class for Physics of the Royal Academy of Science. *Scientific Background on the Nobel Prize in Physics 2010: Graphene*. The Royal Swedish Academy of Sciences. Referred to 20.10.2017.

[15] Papageorgiou, D. G., Kinloch, I. A., Young, R. J. Mechanical properties of graphene and graphene-based nanocomposites. *Prog. Mater. Sci.* **2017**, 90, 75-127.

[16] Zhu, Y., Murali, S., Cai, W., Li, X., Suk, J. W., Potts, J. R., Ruoff, S. R. Graphene and graphene oxide: synthesis, properties and applications. *Adv. Mat.* **2010** 22, 3906-3924.

[17] Suk, J. W., Piner, R. D., An, J., Ruoff, R. S. Mechanical Properties of Monolayer Graphene Oxide. *ACS Nano* **2010**, 4, 6557-6564.

[18] Nag, A., Mitra, A., Mukhopadhyay, S. C. Graphene and its sensor-based applications: A review. *Sens. Actuators A* **2018**, 270, 177-194.

[19] Castro Neto, A. H., Guinea, F., Peres, N. M. R., Novoselov, K. S., Geim, A. K. The electronic properties of graphene. *Review of Modern Physics* **2009**, 81, 109-155.

[20] Falkovsky, L.A. Optical properties of graphene. *Journal of Physics: Conference Series* **2008**, 129.

[21] Liu, G., Teweldebrhan, D, Balandin, A. A. Tuning of graphene properties via controlled exposure to electron beams. *IEEE Transactions on Nanotechnology* **2010**, 10, 865-870.

[22] Li, P., Zhang, B., Cui, T. TiO2 and shrink induced tunable nano self-assembled graphene composites for label-free biosensors. *Sensors and Actuators B* **2015**, 216, 337-342.

[23] Chang, H., Tang, L., Wang, Y., Jiang, J., Li, J. Graphene fluorescence resonance energy transfer aptasensor for the thrombin detection. *Anal. Chem.* **2010**, 82, 2341-2346.

[24] Novikov, S., Lebedeva, N., Satrapinski, A. Ultrasensitive NO_2 gas sensor based on epitaxial graphene. *Journal of Sensors* **2015**, 2015, 1-7.

[25] Lui, C. H., Liu, L., Mak, K. F., Flynn, G. W., Heinz, T. F. Ultraflat graphene. *Nature* **2009**, 462, 339-341.

[26] Wang, X., You, H., Liu, F., Li, M., Wan, L., Li, S., Li, Q., Xu, Y., Tian, R., Yu, Z., Xiang, D., Cheng, J. Large-Scale Synthesis of Few-Layered Graphene using CVD. *Chem. Vap. Deposition* **2009**, 15, 53-56.

[27] Li, X., Cai, W., An, J., Kim, S., Nah, J., Yang, D., Piner, R., Velamakanni, A., Jung, I., Tutuc, E., Banerjee, S. K., Colombo, L., Ruoff, R. S. Large-Area Synthesis of High-Quality and Uniform Graphene Films on Copper Foils. *Science* **2009**, 324, 1312-1314.

[28] Amiri, A., Zubir, M. N. M., Dimiev, A. M., Teng, K. H., Shanbedi, M., Kazi, S. N., Bin Rozali, S. Facile, environmentally friendly, cost effective and scalable production of few-layered graphene. *Chem Eng J.* **2017**, 326, 1105-1115.

[29] Nicolosi, V., Chhowalla, M., Kanatzidis, M. G., Strano, M. S., Coleman, J. N. Liquid exfoliation of layered materials. *Science* **2013**, 340, 1421-1439.

[30] Österholm, A., Kauppila, J., Damlin, P., Kvarnström, C. Electrochemical incorporation of graphene oxide into conducting polymer films. *Electrochimica Acta* **2012**, 83, 463-470.

[31] Lotya, M., King, P. J., Khan, U., De, S., Coleman, J. N. High-concentration, Surfactant-stabilised Graphene Dispersions. *ACS Nano* **2010**, 4, 3155-3162.

[32] Moon, Y. S., Kim, D., Lee, G., Hong, S. Y., Kim, K. L., Park, S. M., Ha, J. S. Fabrication of flexible micro-supercapacitator array with patterned graphene foam/MWNT-COOH/MnOx electrodes and its application. *Carbon* **2015**, 81, 29-37.

[33] Fan, Z., Zhao, Q., Li, T., Yan, J., Ren, Y., Feng, J., Wei, T. Easy synthesis of porous graphene nanosheets and their use in supercapacitors. *Carbon* **2012**, 50, 1699-1712.

[34] Xu, P., Yang, K., Zhou, Z., Shen, P. Porous graphene: properties, preparation, and potential applications. *Chinese Science Bulletin* **2012**, 57, 2948-2955.

[35] Fahimi, A., Jurewicz, I., Smith, R. J., Sharrock, C. S., Bradely, D. A., Henley, S. J., Coleman, J. N., Dalton, A. B. Density controlled conductivity of pristine graphene films. *Carbon* **2013**, 64, 435-443.

[36] Paton, K. R et al. Scalable production of large quantities of defect-free few-layer graphene by shear exfoliation in liquids. *Nat. Mater*. **2014**, 13, 624-630.

[37] Liu, L., Shen, Z., Yi, M., Zhang, X., Ma, S. A green, rapid and size-controlled production of high-quality graphene sheets by hydrodynamic forces. *RSC Advances* **2014**, 36464-36470.

[38] Dispersing head for homogenizer. https://www.labnet.fi/fi/tuote/v109695/109695/dispersing-heads-for-homogeniser-polytron/542850/1. Referred to 17.08.2018.

[39] Khan, U., Porwal, H., O'Neill, A., Nawaz, K., May, P., Coleman, J. N. Solvent-Exfoliated Graphene at Extremely High Concentration. *Langmuir* **2011**, 27, 9077-9082.

[40] Wang, S., Wang, C., Ji, X., Lin, M. Surfactant- and sonication- free exfoliation approach to aqueous graphene dispersion. *Mater. Lett.* **2018**, 217, 67-70.

[41] Lin, S., Blankschtein, D. Role of the Bile Salt Surfactant Sodium Cholate in Enhancing the Aqueous Dispersion Stability of Single-Walled Carbon Nanotubes: A Molecular Dynamics Simulation Study. *J. Phys. Chem. B* **2010**, 114, 15616-15625.

[42] Shih, C-J., Paulus, G. L. C., Wang, Q. H., Jin, Z., Blankschtein, D., Strano, M. Understanding Surfactant/Graphene Interactions Using a Graphene Field Effect Transistor: Relating Molecular Structure to Hysteresis and Carrier Mobility. *Langmuir* **2012**, 28, 8579-8586.

[43] Yi, M., Shen, Z. Kitchen blender for producing high-quality few-layer graphene. *Carbon* **2014**, 78, 622-626.

[44] Goldstein, J. I., Newbury, D. E., Michael, J. R., Ritchie, N. W. M., Scott, J. H. J, Joy, D. C. Scanning Electron Microscopy and X-Ray Microanalysis. Springer Nature, New York, p. 2, **2018**.

[45] Stankovich, SD., Dikin, D. A., Dommett, G. H. B., Kohlhaas, K. M., Zimney, E. J., Stach, E. A., Piner, R. D., Nguyen, S. T., Ruoff, R. S. Graphene-based composite materials. *Nature Lett* **2006**, 442, 282-286.

[46] Stoller, M. D., Park, S., Zhu, Y., An, J., Ruoff, R. S. Graphene-based ultracapacitors. *Nano Lett.* **2008**, 8, 3498-3502.

[47] Mehta, Rahul. Interactions, Imaging and Spectra in SEM. https://www.intechopen.com/books/scanning-electron-microscopy/interactions-imaging-spectra-in-sem p. 22. Referred to 10.08.2018.

[48] Illakkiya, J. T., Rajalakshmi, P. U., Oommen, R. Nebulized spray pyrolysis: a new method for synthesis of graphene film and their characteristics. *Surf. Coat. Technol.* **2016**, 307, 65-72.

[49] RCF values for the Hermle Z200A centrifuge. https://gsecars.uchicago.edu/sites/gsecars.uchicago.edu/files/uploads/HermleZ200A%20Instruction_Manual.pdf, p 14. Referred to 16.08.2018.

[50] Chabot, V., Kim, B., Sloper, B., Tzoganakis, C., Yu, A. High yield production and purification of few layer graphene by Gum Arabic assisted physical sonication. *Sci. Rep.* **2013**, 3, 1-7.

[51] Kauppila, J., Lund, S. FENNOFLAKES: A Summary of the High-shear Exfoliation of Graphite. Åbo Akademi **2016**, 7.

[52] Pierce: Sodium cholate. Product information and instructions. http://solioz-scientific.ch/knowledge/Sodium_cholate.pdf. Referred to 22.02.2018.

[53] Lotya, M., King, P. J., Khan, U., De, S., Coleman, J. N. High-concentration, Surfactant-stabilised Graphene Dispersions. *ACS Nano* **2010**, 4, 3155-3162.

[54] Eriksson, F. Yt- och kolloidkemi. Fysikalisk kemi, Åbo Akademi **2007**, 69.

[55] Kauppila, J., Lund, S. FENNOFLAKES: A Summary of the High-shear Exfoliation of Graphite. Åbo Akademi **2016**, 4.

[56] Lotya, M., Hernandez, Y., King, P. J., Smith, R. J., Nicolosi, V., Karlsson, L. S., Blighe, F. M., De, S., Wang, Z., McGovern, I. T., Dyesberg, G. S., Coleman, J. N. Liquid Phase Production of Graphene by Exfoliation of Graphite in Surfactant/Water Solutions. *J. Am. Chem. Soc.* **2009**, 131, 3611-3620.

[57] Chun, S., Choi, Y., Park, W. All-graphene strain sensor on soft substrate. *Carbon* **2017**, 116, 753-759.

[58] Electrical conductivity of common materials. https://www.engineeringtoolbox.com/conductors-d_1381.html. Referred to 20.08.2018.

[59] Su, C.-Y., Lu, A.-Y., Xu, Y., Chen, F.-R., Khlobystov, A. N., Li, L.-J. High-Quality Thin Graphene Films from Fast Electrochemical Exfoliation. *ACS Nano*, **2011**, 5, 2332-2339.

[60] Xia, F., Mueller, T., Li, Y-m., Valdes-Garcia, A., Avouris, P. Ultrafast graphene photodetector. *Nat. Nanotechnol*. **2009**, 4, 839.

[61] Mulero. A., Parra, M. I., Cachadiña, I. The Somayajulu correlation for the surface tension revisited. *Fluid Ph. Equilibria* **2013**, 339, 81-88.

[62] Fischbein, M. D., Drndić, M. Electron beam nanosculpting of suspended graphene sheets. *Appl Phys Lett* **2008**, 93, 1-11.

Appendix A

Summary of experiment series

Nr of samples/ batch	Test series title / aim of experiment	Centrif. speed rpm	Centrif. time / sample (min)	Mixing time min	Graphite conc. mg/ml	Stab. time points, days	Batches used
5	Centr. speed	1500-6000	30	30	20	0,3,7	Sigma Aldrich (SA)
5	Centr. time	1500	30-150	30	20	0,7	SA
3	Time vs. speed 1	1500	60-120	30	20	0,3,7	SA & #6
3	Time vs. speed 2	2500	60-120	30	20	0,3,7	SA & #6
3	Time vs. speed 3	750	60-120	30	20	0,3,7	SA & #6
3	Time vs. speed for Alfa Aesar (AA) and #3	1500	60-120	30	20	0,4,7	AA & #3
3	Repeatability 1	500	60	30	20	0,2,7	#6
3	Repeatability 2	500	60	30	20	0	#3
3	Repeatability series 3	1500	60	30	20	0,2,7	#6
3	Repeatability series 4	1500	60	30	20	0,2,7	#3
5	SC series	1500	60	30	20	0,2,7	#6
5	SC series, additional measurements	1500	60	30	20	0,2	#6
1	Samples for SEM	1500	60	30	20	0	One of each batch
7	Exfoliation time	1500	60	15-240	20	0,2,7	#6
4	Graphite concentration	1500	60	30	50-200	0,2,7	#6
4	Graphite conc. with PT 10-35 (bigger mixer)	1500	60	30	50-200	0	AA
1	Maximum graphene conc.	1500	60	240	200	0	AA
1	Film fabrication tests with wk 24 graphene dispersion	-	-	-	-	-	AA

Appendix B

EDX spectrum of a graphene dispersion fabricated with the Finnish graphite #6 on an Al-substrate

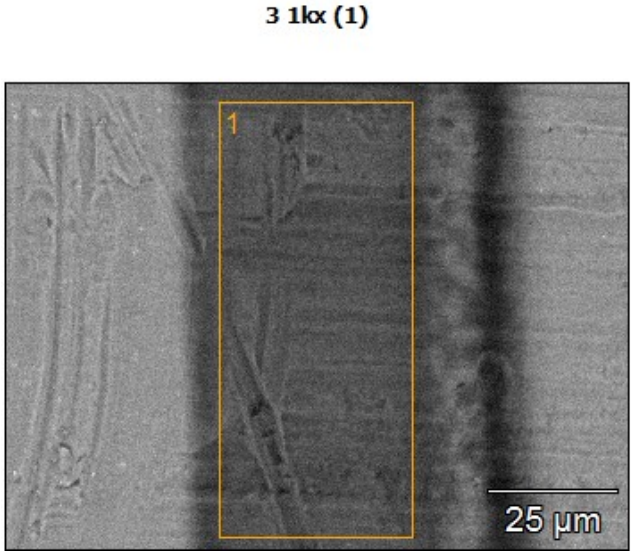

Image Name:	3 1kx (1)
Image Resolution:	1024 by 768
Image Pixel Size:	0.12 µm
Acc. Voltage:	15.0 kV
Magnification:	1000

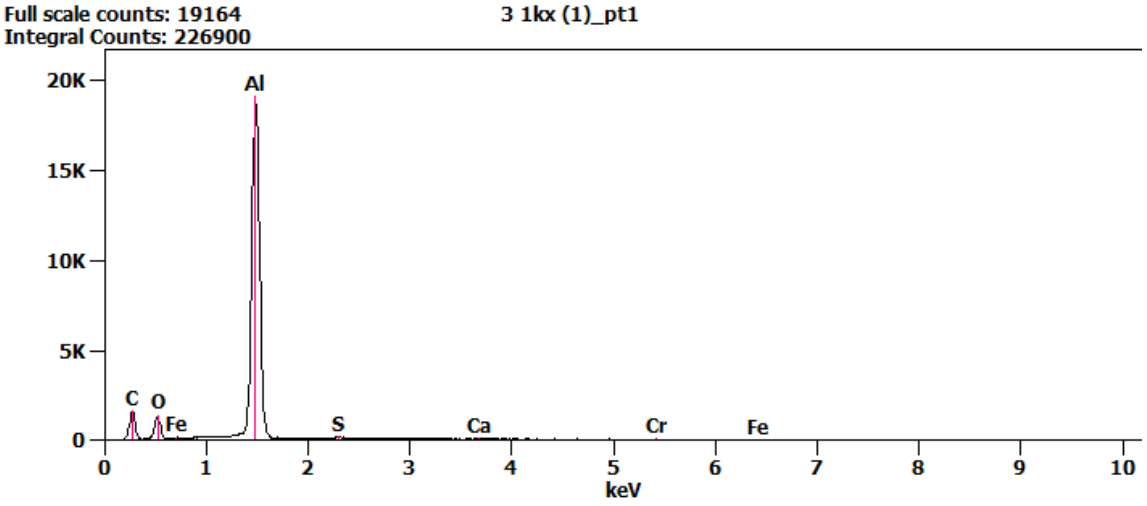

Weight %

	C-K	O-K	Al-K	S-K	Ca-K	Cr-K	Fe-K
3 1kx (1)_pt1	36.73	14.58	47.34	0.47	0.15	0.22	0.52

Weight % Error (+/- 1 Sigma)

	C-K	O-K	Al-K	S-K	Ca-K	Cr-K	Fe-K
3 1kx (1)_pt1	±0.99	±0.17	±0.15	±0.03	±0.03	±0.05	±0.08

Atom %

	C-K	O-K	Al-K	S-K	Ca-K	Cr-K	Fe-K
3 1kx (1)_pt1	53.13	15.83	30.48	0.26	0.07	0.07	0.16

Atom % Error (+/- 1 Sigma)

	C-K	O-K	Al-K	S-K	Ca-K	Cr-K	Fe-K
3 1kx (1)_pt1	±1.43	±0.19	±0.09	±0.01	±0.01	±0.02	±0.03

Formula

	C-K	O-K	Al-K	S-K	Ca-K	Cr-K	Fe-K
3 1kx (1)_pt1	C	O	Al	S	Ca	Cr	Fe

Compound %

	C	O	Al	S	Ca	Cr	Fe
3 1kx (1)_pt1	36.73	14.58	47.34	0.47	0.15	0.22	0.52

Appendix C

EDX spectrum of a graphene dispersion fabricated with the Finnish graphite #3 on an Al-substrate

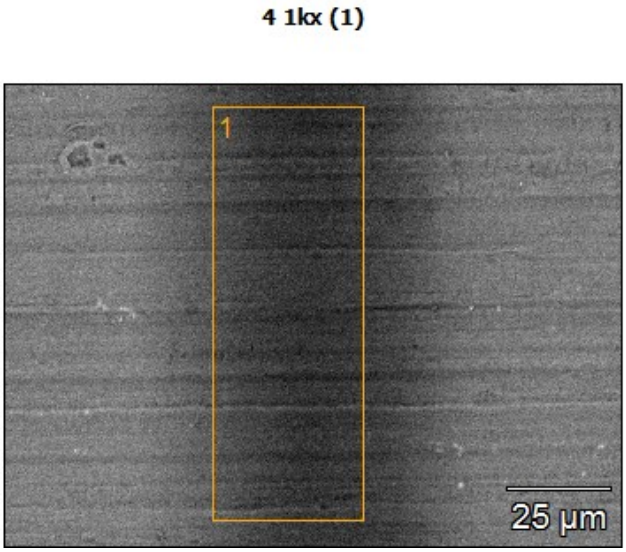

Image Name:	4 1kx (1)
Image Resolution:	1024 by 768
Image Pixel Size:	0.15 µm
Acc. Voltage:	15.0 kV
Magnification:	808

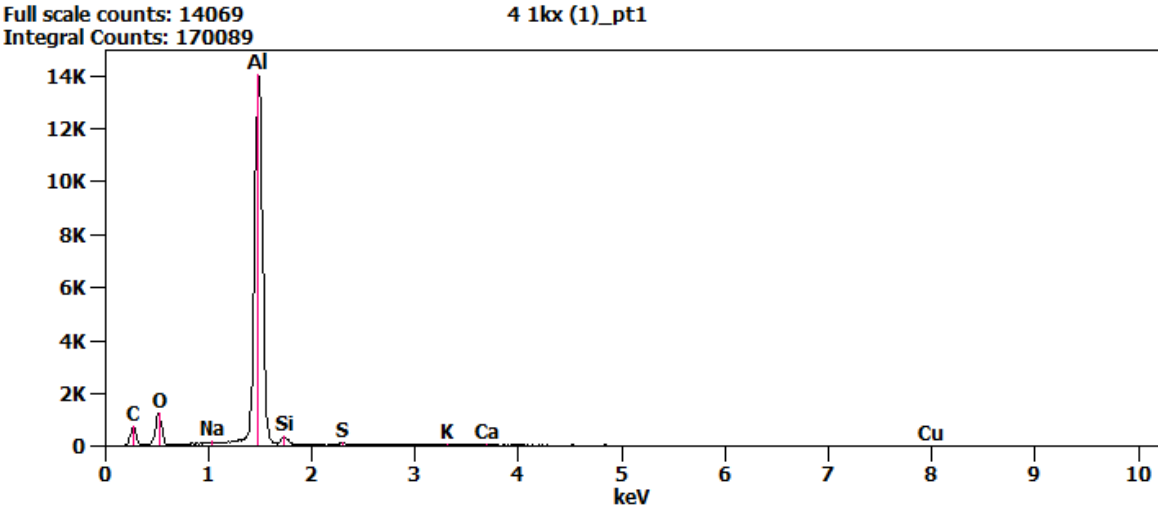

Weight %

	C-K	O-K	Na-K	Al-K	Si-K	S-K	K-K	Ca-K	Cu-K
4 1kx (1)_pt1	27.44	18.76	0.19	50.59	1.39	0.47	0.44	0.34	0.39

Weight % Error (+/- 1 Sigma)

	C-K	O-K	Na-K	Al-K	Si-K	S-K	K-K	Ca-K	Cu-K
4 1kx (1)_pt1	±0.80	±0.26	±0.03	±0.18	±0.10	±0.03	±0.04	±0.04	±0.17

Atom %

	C-K	O-K	Na-K	Al-K	Si-K	S-K	K-K	Ca-K	Cu-K
4 1kx (1)_pt1	42.07	21.60	0.15	34.53	0.91	0.27	0.21	0.16	0.11

Atom % Error (+/- 1 Sigma)

	C-K	O-K	Na-K	Al-K	Si-K	S-K	K-K	Ca-K	Cu-K
4 1kx (1)_pt1	±1.22	±0.29	±0.03	±0.12	±0.06	±0.02	±0.02	±0.02	±0.05

Formula

	C-K	O-K	Na-K	Al-K	Si-K	S-K	K-K	Ca-K	Cu-K
4 1kx (1)_pt1	C	O	Na	Al	Si	S	K	Ca	Cu

Compound %

	C	O	Na	Al	Si	S	K	Ca	Cu
4 1kx (1)_pt1	27.44	18.76	0.19	50.59	1.39	0.47	0.44	0.34	0.39

Appendix D

EDX spectrum of a graphene dispersion fabricated with the Finnish graphite #6 on copper substrate

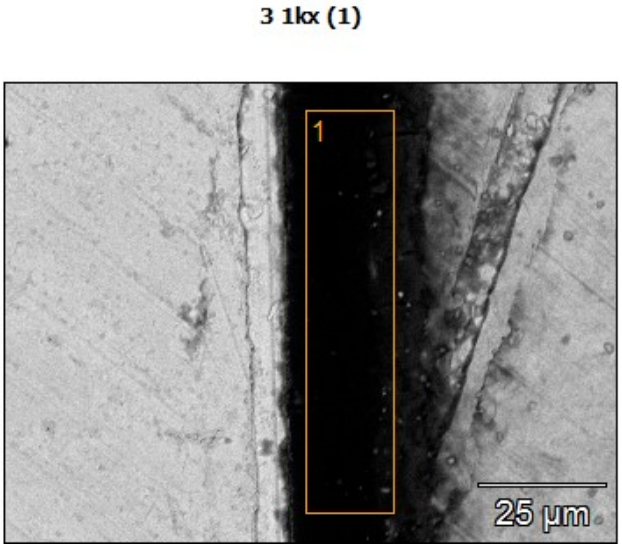

Image Name:	3 1kx (1)
Image Resolution:	1024 by 768
Image Pixel Size:	0.12 µm
Acc. Voltage:	15.0 kV
Magnification:	1000

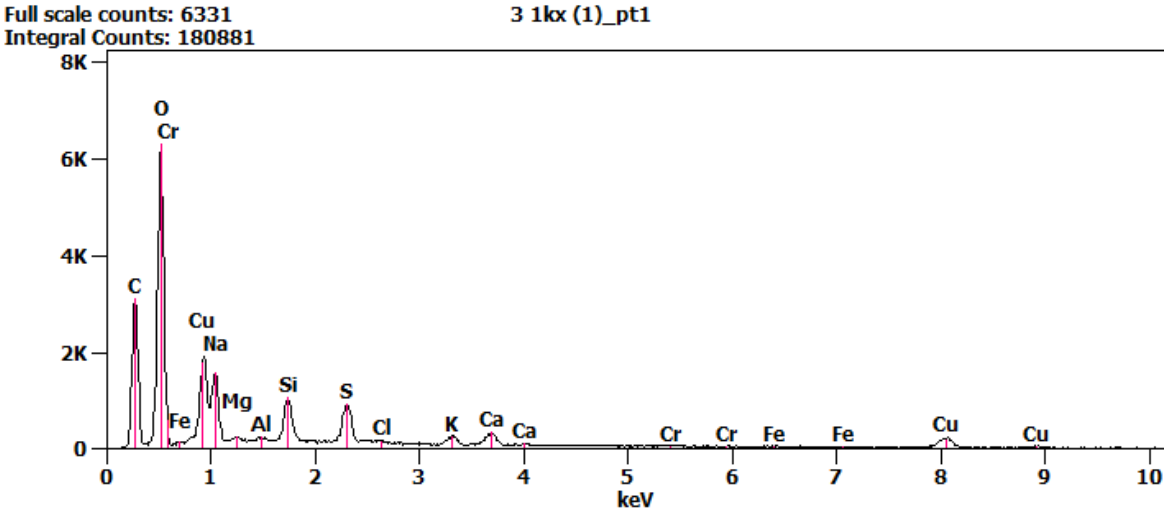

Weight %

	C-K	O-K	Na-K	Mg-K	Al-K	Si-K	S-K	Cl-K	K-K	Ca-K	Cr-K	Fe-K
3 1kx (1)_pt1	30.81	52.24	6.90	0.20	0.19	2.70	3.30	0.26	1.01	1.78	0.33	0.28

Weight % Error (+/- 1 Sigma)

	C-K	O-K	Na-K	Mg-K	Al-K	Si-K	S-K	Cl-K	K-K	Ca-K	Cr-K	Fe-K
3 1kx (1)_pt1	±0.81	±0.45	±0.20	±0.03	±0.03	±0.05	±0.07	±0.03	±0.08	±0.10	±0.06	±0.09

Atom %

	C-K	O-K	Na-K	Mg-K	Al-K	Si-K	S-K	Cl-K	K-K	Ca-K	Cr-K	Fe-K
3 1kx (1)_pt1	39.87	50.75	4.67	0.13	0.11	1.50	1.60	0.11	0.40	0.69	0.10	0.08

Atom % Error (+/- 1 Sigma)

	C-K	O-K	Na-K	Mg-K	Al-K	Si-K	S-K	Cl-K	K-K	Ca-K	Cr-K	Fe-K
3 1kx (1)_pt1	±1.05	±0.44	±0.13	±0.02	±0.01	±0.03	±0.04	±0.01	±0.03	±0.04	±0.02	±0.03

Formula

	C-K	O-K	Na-K	Mg-K	Al-K	Si-K	S-K	Cl-K	K-K	Ca-K	Cr-K	Fe-K
3 1kx (1)_pt1	C	O	Na	Mg	Al	Si	S	Cl	K	Ca	Cr	Fe

Compound %

	C	O	Na	Mg	Al	Si	S	Cl	K	Ca	Cr	Fe
3 1kx (1)_pt1	30.81	52.24	6.90	0.20	0.19	2.70	3.30	0.26	1.01	1.78	0.33	0.28

Appendix E

EDX spectrum of a graphene dispersion fabricated with the Finnish graphite #6 on copper substrate

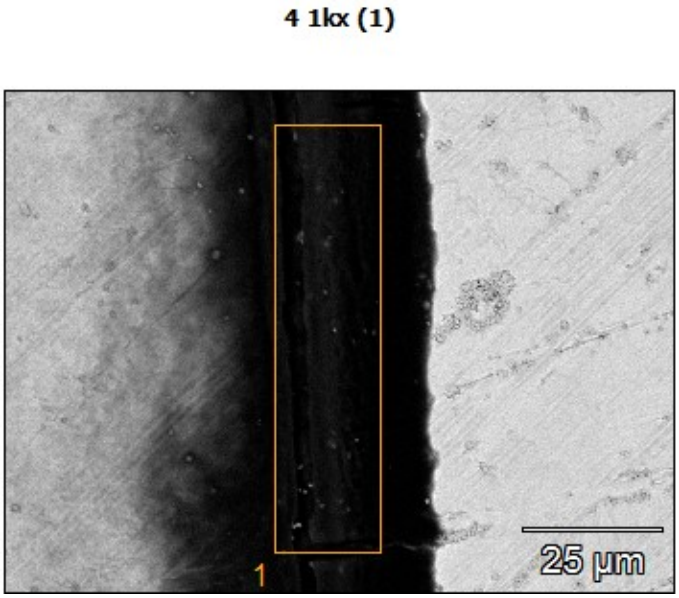

Image Name:	4 1kx (1)
Image Resolution:	1024 by 768
Image Pixel Size:	0.12 µm
Acc. Voltage:	15.0 kV
Magnification:	1000

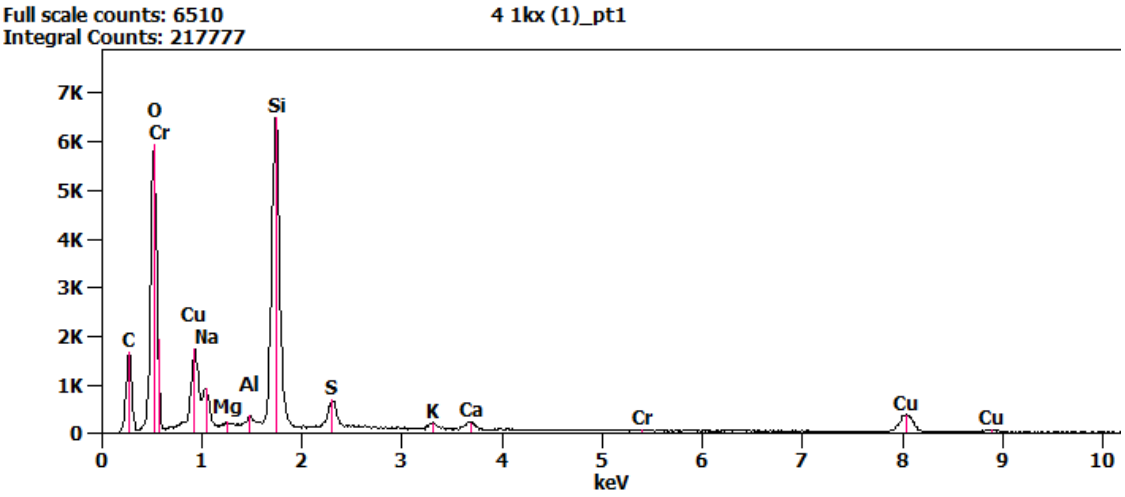

Weight %

	C-K	O-K	Na-K	Mg-K	Al-K	Si-K	S-K	K-K	Ca-K	Cr-K
4 1kx (1)_pt1	30.67	39.65	4.23	0.17	0.43	19.81	2.80	0.62	1.13	0.49

Weight % Error (+/- 1 Sigma)

	C-K	O-K	Na-K	Mg-K	Al-K	Si-K	S-K	K-K	Ca-K	Cr-K
4 1kx (1)_pt1	±0.84	±2.06	±0.09	±0.03	±0.03	±0.10	±0.08	±0.04	±0.05	±0.07

Atom %

	C-K	O-K	Na-K	Mg-K	Al-K	Si-K	S-K	K-K	Ca-K	Cr-K
4 1kx (1)_pt1	41.96	40.73	3.03	0.11	0.26	11.59	1.44	0.26	0.46	0.16

Atom % Error (+/- 1 Sigma)

	C-K	O-K	Na-K	Mg-K	Al-K	Si-K	S-K	K-K	Ca-K	Cr-K
4 1kx (1)_pt1	±1.15	±2.12	±0.06	±0.02	±0.02	±0.06	±0.04	±0.02	±0.02	±0.02

Formula

	C-K	O-K	Na-K	Mg-K	Al-K	Si-K	S-K	K-K	Ca-K	Cr-K
4 1kx (1)_pt1	C	O	Na	Mg	Al	Si	S	K	Ca	Cr

Compound %

	C	O	Na	Mg	Al	Si	S	K	Ca	Cr
4 1kx (1)_pt1	30.67	39.65	4.23	0.17	0.43	19.81	2.80	0.62	1.13	0.49

Appendix F

Additional EDX spectra for Alfa Aesar graphite

AA 200x (1)

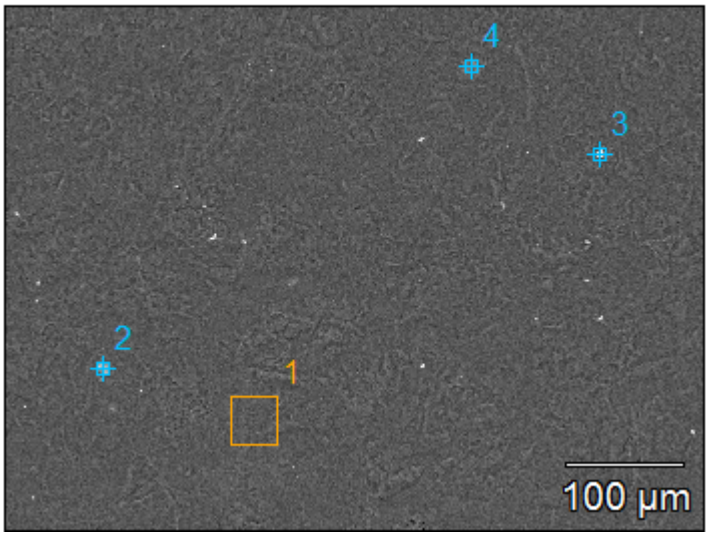

Image Name:	AA 200x (1)
Image Resolution:	1024 by 768
Image Pixel Size:	0.59 µm
Acc. Voltage:	20.0 kV
Magnification:	200

Full scale counts: 5353
Integral Counts: 46985

AA 200x (1)_pt1

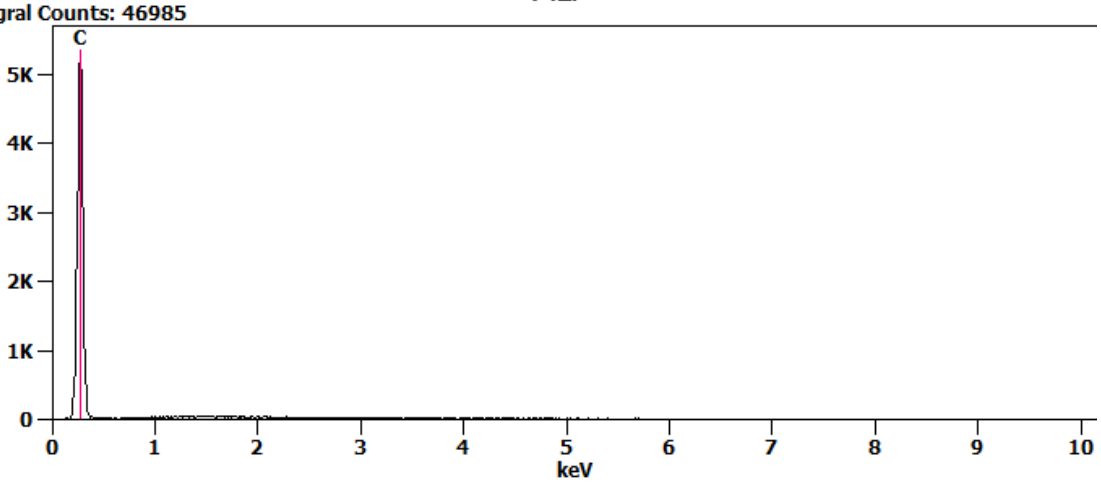

Full scale counts: 5551
Integral Counts: 130358

AA 200x (1)_pt2

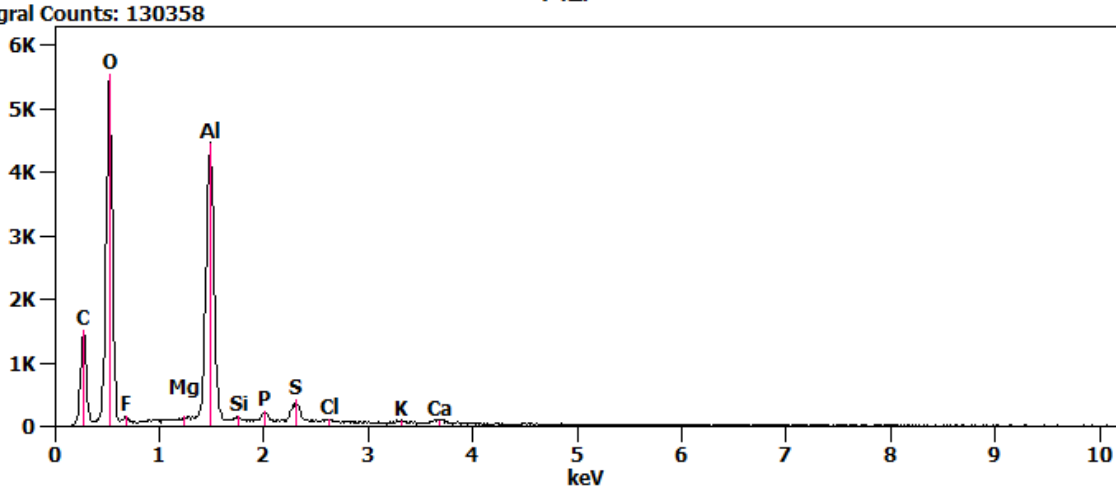

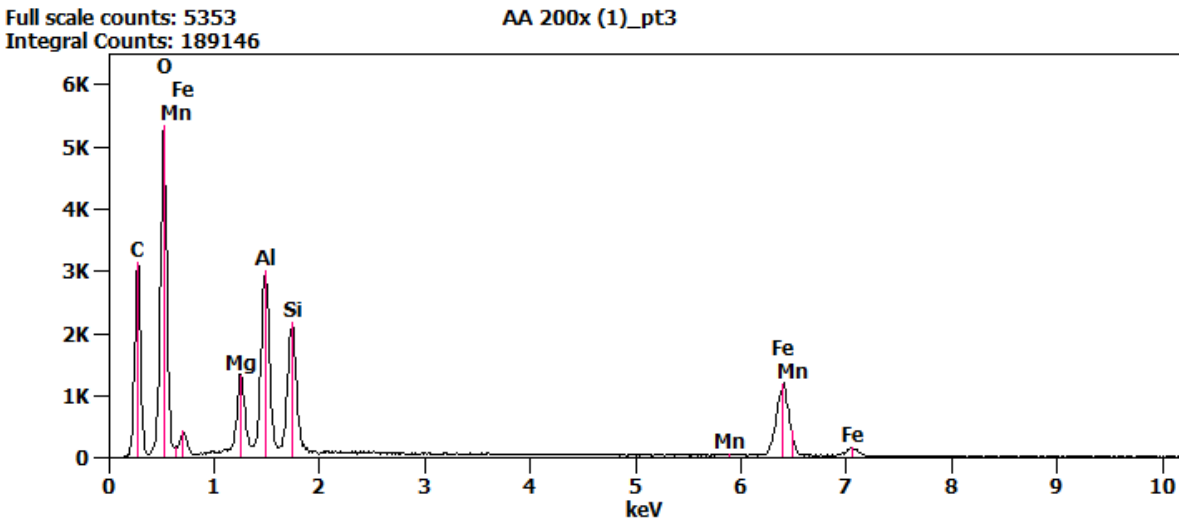
Full scale counts: 5353
Integral Counts: 189146
AA 200x (1)_pt3
O
Fe
Mn
C
Al
Si
Mg
Fe
Mn
Mn
Fe
6K
5K
4K
3K
2K
1K
0
0 1 2 3 4 5 6 7 8 9 10
keV

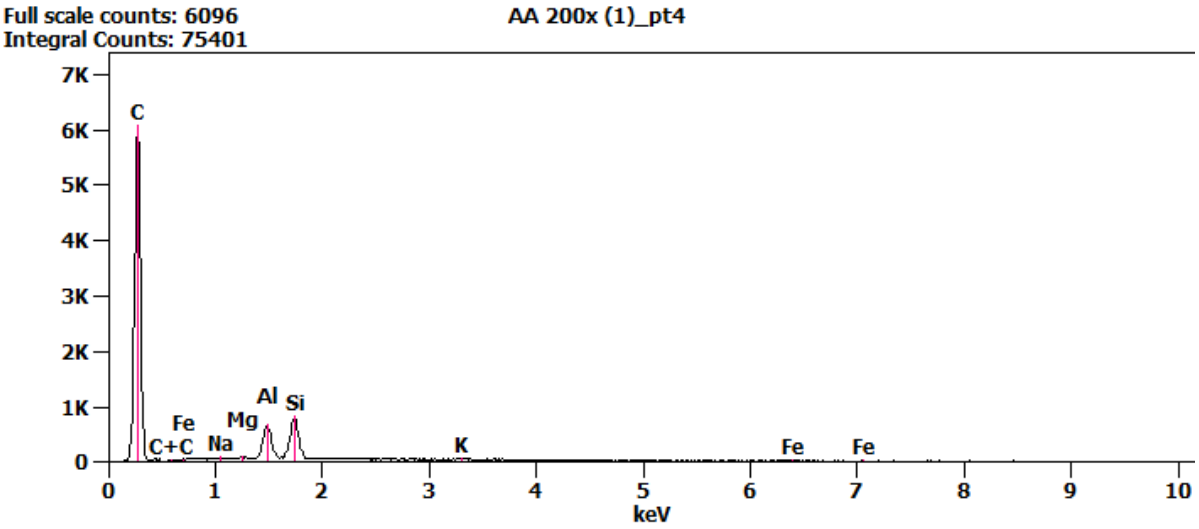
Full scale counts: 6096
Integral Counts: 75401
AA 200x (1)_pt4
C
Fe
C+C
Na
Mg
Al
Si
K
Fe
Fe
7K
6K
5K
4K
3K
2K
1K
0
0 1 2 3 4 5 6 7 8 9 10
keV

Weight %

	C-K	O-K	F-K	Na-K	Mg-K	Al-K	Si-K	P-K	S-K	Cl-K	K-K	Ca-K	Mn-K	Fe-K
AA 200x (1)_pt1	100.00													
AA 200x (1)_pt2	26.18	57.60	1.40		0.10	12.30	0.17	0.47	1.24	0.15	0.14	0.25		
AA 200x (1)_pt3	34.19	42.32			2.54	5.78	4.43						0.20	10.55
AA 200x (1)_pt4	92.19			0.23	0.11	2.81	4.00				0.34			0.32

Weight % Error (+/- 1 Sigma)

	C-K	O-K	F-K	Na-K	Mg-K	Al-K	Si-K	P-K	S-K	Cl-K	K-K	Ca-K	Mn-K	Fe-K
AA 200x (1)_pt1	±2.57													
AA 200x (1)_pt2	±0.71	±0.51	±0.26		±0.03	±0.08	±0.02	±0.05	±0.03	±0.02	±0.02	±0.04		
AA 200x (1)_pt3	±0.90	±0.39			±0.05	±0.08	±0.06						±0.03	±0.14
AA 200x (1)_pt4	±2.37			±0.04	±0.03	±0.09	±0.09				±0.03			±0.09

Atom %

	C-K	O-K	F-K	Na-K	Mg-K	Al-K	Si-K	P-K	S-K	Cl-K	K-K	Ca-K	Mn-K	Fe-K
AA 200x (1)_pt1	100.00													
AA 200x (1)_pt2	34.13	56.37	1.15		0.07	7.13	0.10	0.24	0.61	0.06	0.05	0.10		
AA 200x (1)_pt3	46.21	42.93			1.70	3.48	2.56						0.06	3.07
AA 200x (1)_pt4	96.53			0.13	0.06	1.31	1.79				0.11			0.07

Atom % Error (+/- 1 Sigma)

	C-K	O-K	F-K	Na-K	Mg-K	Al-K	Si-K	P-K	S-K	Cl-K	K-K	Ca-K	Mn-K	Fe-K
AA 200x (1)_pt1	±2.57													
AA 200x (1)_pt2	±0.93	±0.50	±0.21		±0.02	±0.05	±0.01	±0.02	±0.01	±0.01	±0.01	±0.02		
AA 200x (1)_pt3	±1.21	±0.40			±0.04	±0.05	±0.03						±0.01	±0.04
AA 200x (1)_pt4	±2.48			±0.02	±0.02	±0.04	±0.04				±0.01			±0.02

Formula

	C-K	O-K	F-K	Na-K	Mg-K	Al-K	Si-K	P-K	S-K	Cl-K	K-K	Ca-K	Mn-K	Fe-K
AA 200x (1)_pt1	C													
AA 200x (1)_pt2	C	O	F		Mg	Al	Si	P	S	Cl	K	Ca		
AA 200x (1)_pt3	C	O			Mg	Al	Si						Mn	Fe
AA 200x (1)_pt4	C			Na	Mg	Al	Si				K			Fe

Compound %

	C	O	F	Na	Mg	Al	Si	P	S	Cl	K	Ca	Mn	Fe
AA 200x (1)_pt1	100.00													
AA 200x (1)_pt2	26.18	57.60	1.40		0.10	12.30	0.17	0.47	1.24	0.15	0.14	0.25		
AA 200x (1)_pt3	34.19	42.32			2.54	5.78	4.43						0.20	10.55
AA 200x (1)_pt4	92.19			0.23	0.11	2.81	4.00				0.34			0.32

Appendix G

Additional EDX spectra from Sigma-Aldrich graphite

SA 30x (1)

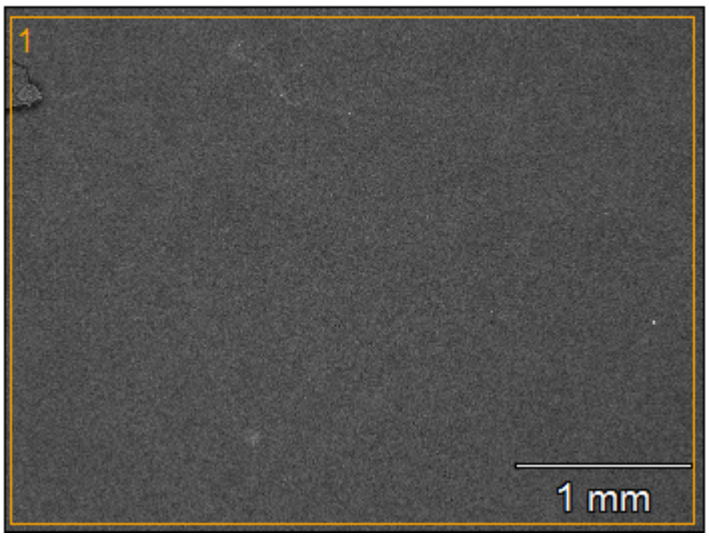

Image Name:	SA 30x (1)
Image Resolution:	1024 by 768
Image Pixel Size:	3.93 µm
Acc. Voltage:	20.0 kV
Magnification:	30

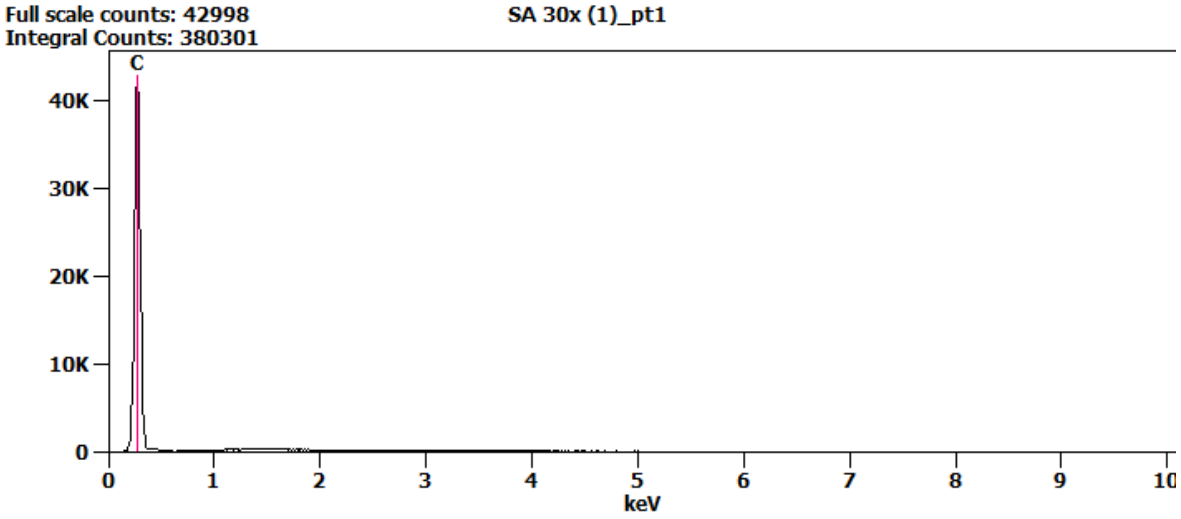

Weight %

	C-K
SA 30x (1)_pt1	100.00

Weight % Error (+/- 1 Sigma)

	C-K
SA 30x (1)_pt1	±2.55

Atom %

	C-K
SA 30x (1)_pt1	100.00

Atom % Error (+/- 1 Sigma)

	C-K
SA 30x (1)_pt1	±2.55

Formula

	C-K
SA 30x (1)_pt1	C

Compound %

	C
SA 30x (1)_pt1	100.00

Appendix H

Additional EDX spectra from SC

SC 200x (1)

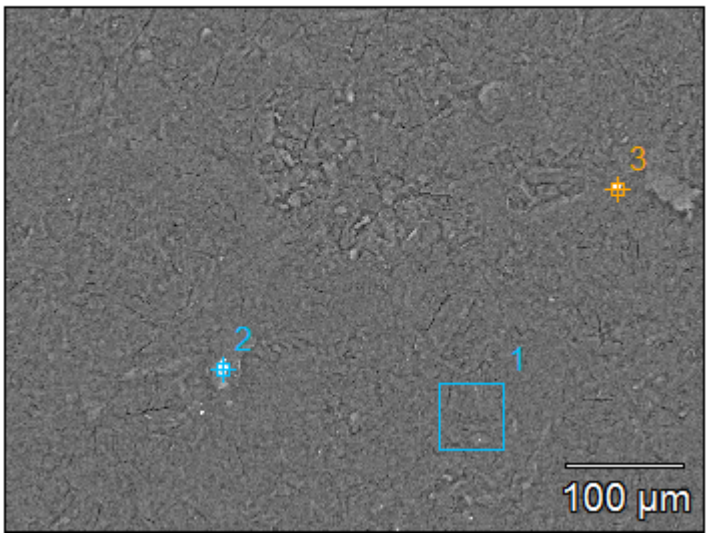

Image Name:	SC 200x (1)
Image Resolution:	1024 by 768
Image Pixel Size:	0.59 µm
Acc. Voltage:	20.0 kV
Magnification:	200

Full scale counts: 5352
Integral Counts: 73545

SC 200x (1)_pt1

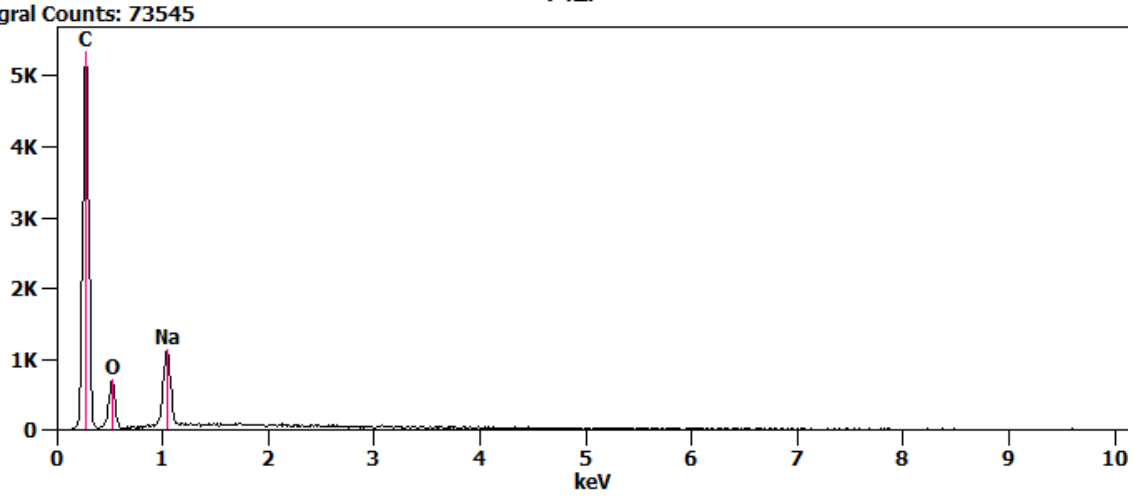

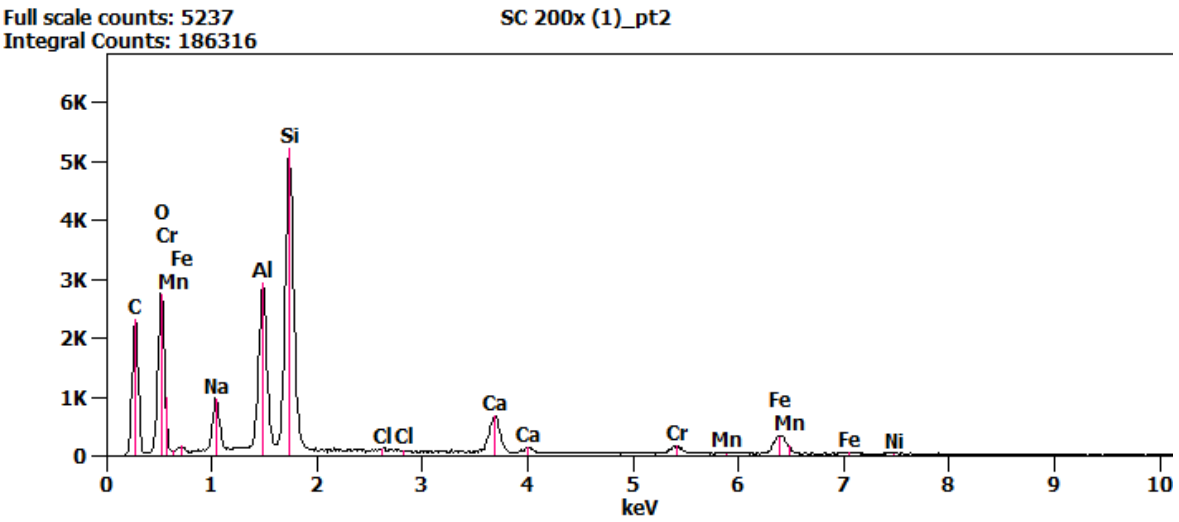
Full scale counts: 5237
Integral Counts: 186316
SC 200x (1)_pt2
6K
5K
4K
3K
2K
1K
0
O
Cr
Fe
Mn
C
Na
Al
Si
Cl Cl
Ca
Ca
Cr
Mn
Fe
Mn
Fe
Ni
0 1 2 3 4 5 6 7 8 9 10
keV

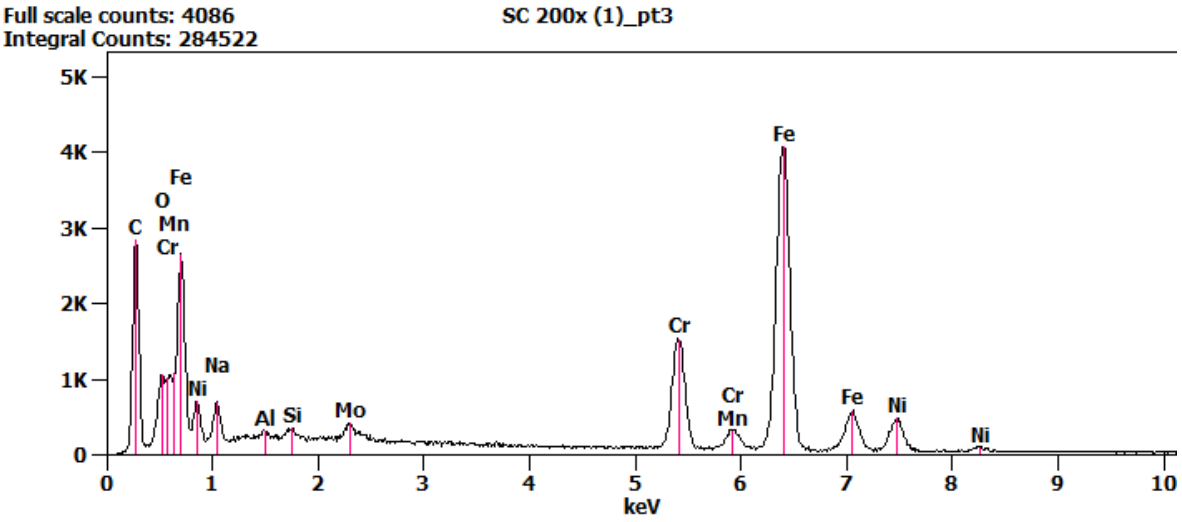
Full scale counts: 4086
Integral Counts: 284522
SC 200x (1)_pt3
5K
4K
3K
2K
1K
0
Fe
O
Mn
Cr
C
Ni
Na
Al
Si
Mo
Cr
Cr
Mn
Fe
Fe
Ni
Ni
0 1 2 3 4 5 6 7 8 9 10
keV

Weight %

	C-K	O-K	Na-K	Al-K	Si-K	Cl-K	Ca-K	Cr-K	Mn-K	Fe-K	Ni-K	Mo-L
SC 200x (1)_pt1	69.02	22.42	8.56									
SC 200x (1)_pt2	37.73	31.78	3.66	6.24	12.05	0.06	2.75	1.08	0.06	4.11	0.48	
SC 200x (1)_pt3	33.25	3.86	3.50	0.21	0.37			9.60	0.70	41.30	6.24	0.98

Weight % Error (+/- 1 Sigma)

	C-K	O-K	Na-K	Al-K	Si-K	Cl-K	Ca-K	Cr-K	Mn-K	Fe-K	Ni-K	Mo-L
SC 200x (1)_pt1	±1.78	±0.41	±0.12									
SC 200x (1)_pt2	±1.02	±0.41	±0.07	±0.07	±0.09	±0.02	±0.06	±0.07	±0.04	±0.13	±0.06	
SC 200x (1)_pt3	±0.91	±0.32	±0.19	±0.03	±0.02			±0.12	±0.14	±0.28	±0.22	±0.09

Atom %

	C-K	O-K	Na-K	Al-K	Si-K	Cl-K	Ca-K	Cr-K	Mn-K	Fe-K	Ni-K	Mo-L
SC 200x (1)_pt1	76.41	18.64	4.95									
SC 200x (1)_pt2	51.32	32.45	2.60	3.78	7.01	0.03	1.12	0.34	0.02	1.20	0.13	
SC 200x (1)_pt3	65.35	5.70	3.59	0.19	0.31			4.36	0.30	17.46	2.51	0.24

Atom % Error (+/- 1 Sigma)

	C-K	O-K	Na-K	Al-K	Si-K	Cl-K	Ca-K	Cr-K	Mn-K	Fe-K	Ni-K	Mo-L
SC 200x (1)_pt1	±1.97	±0.34	±0.07									
SC 200x (1)_pt2	±1.38	±0.42	±0.05	±0.04	±0.05	±0.01	±0.03	±0.02	±0.01	±0.04	±0.02	
SC 200x (1)_pt3	±1.78	±0.48	±0.19	±0.02	±0.02			±0.05	±0.06	±0.12	±0.09	±0.02

Formula

	C-K	O-K	Na-K	Al-K	Si-K	Cl-K	Ca-K	Cr-K	Mn-K	Fe-K	Ni-K	Mo-L
SC 200x (1)_pt1	C	O	Na									
SC 200x (1)_pt2	C	O	Na	Al	Si	Cl	Ca	Cr	Mn	Fe	Ni	
SC 200x (1)_pt3	C	O	Na	Al	Si			Cr	Mn	Fe	Ni	Mo

Compound %

	C	O	Na	Al	Si	Cl	Ca	Cr	Mn	Fe	Ni	Mo
SC 200x (1)_pt1	69.02	22.42	8.56									
SC 200x (1)_pt2	37.73	31.78	3.66	6.24	12.05	0.06	2.75	1.08	0.06	4.11	0.48	
SC 200x (1)_pt3	33.25	3.86	3.50	0.21	0.37			9.60	0.70	41.30	6.24	0.98